immunohistochemical staining using human-specific hCK8/18 mouse monoclonal antibodies (NCL5D3; MP Biomedicals, Aurora, OH) or BrdU mouse monoclonal antibodies (Bu20a; Dako Cytomation, Glostrup, Denmark). The antibodies were visualized with a Vectastain ABC Kit (Vector Laboratories, Burlingame, CA) using DAB substrates.

SUPPLEMENTAL INFORMATION

Supplemental Information includes Extended Experimental Procedures, four figures, and five tables and can be found with this article online at http://dx.doi.org/10.1016/j.celrep.2012.08.009.

LICENSING INFORMATION

ACKNOWLEDGMENTS

We thank Jean-Louis Guenet for helpful discussion. This study was supported in part by a Grant-in-Aid for Research on New Drug Development from the Ministry of Health, Labor and Welfare of Japan, and by the Industrial Technology Research Grant Program in 2008, New Energy, and the Industrial Technology Development Organization of Japan.

Received: October 26, 2011
Revised: May 8, 2012
Accepted: August 9, 2012
Published online: September 13, 2012

REFERENCES

Azuma, H., Paulk, N., Ranade, A., Dorrell, C., Al-Dhalimy, M., Ellis, E., Strom, S., Kay, M.A., Finegold, M., and Grompe, M. (2007). Robust expansion of human hepatocytes in Fah-/-/Rag2-/-/Il2rg-/- mice. Nat. Biotechnol. *25*, 903–910.

Baiocchi, M., Biffoni, M., Ricci-Vitiani, L., Pilozzi, E., and De Maria, R. (2010). New models for cancer research: human cancer stem cell xenografts. Curr. Opin. Pharmacol. *10*, 380–384.

Bosma, G.C., Custer, R.P., and Bosma, M.J. (1983). A severe combined immunodeficiency mutation in the mouse. Nature *301*, 527–530.

Brehm, M.A., Shultz, L.D., and Greiner, D.L. (2010). Humanized mouse models to study human diseases. Curr. Opin. Endocrinol. Diabetes Obes. *17*, 120–125.

Cui, X., Ji, D., Fisher, D.A., Wu, Y., Briner, D.M., and Weinstein, E.J. (2011). Targeted integration in rat and mouse embryos with zinc-finger nucleases. Nat. Biotechnol. *29*, 64–67.

Denton, P.W., and García, J.V. (2011). Humanized mouse models of HIV infection. AIDS Rev. *13*, 135–148.

Finnie, N.J., Gottlieb, T.M., Blunt, T., Jeggo, P.A., and Jackson, S.P. (1995). DNA-dependent protein kinase activity is absent in xrs-6 cells: implications for site-specific recombination and DNA double-strand break repair. Proc. Natl. Acad. Sci. USA *92*, 320–324.

Franco, S., Alt, F.W., and Manis, J.P. (2006). Pathways that suppress programmed DNA breaks from progressing to chromosomal breaks and translocations. DNA Repair (Amst.) *5*, 1030–1041.

Gao, Y., Chaudhuri, J., Zhu, C., Davidson, L., Weaver, D.T., and Alt, F.W. (1998). A targeted DNA-PKcs-null mutation reveals DNA-PK-independent functions for KU in V(D)J recombination. Immunity *9*, 367–376.

Geurts, A.M., Cost, G.J., Freyvert, Y., Zeitler, B., Miller, J.C., Choi, V.M., Jenkins, S.S., Wood, A., Cui, X., Meng, X., et al. (2009). Knockout rats via embryo microinjection of zinc-finger nucleases. Science *325*, 433.

Gustafsson, E., Mattsson, A., Holmdahl, R., and Mattsson, R. (1994). Pregnancy in B-cell-deficient mice: postpartum transfer of immunoglobulins prevents neonatal runting and death. Biol. Reprod. *51*, 1173–1180.

Ishikawa, F., Yasukawa, M., Lyons, B., Yoshida, S., Miyamoto, T., Yoshimoto, G., Watanabe, T., Akashi, K., Shultz, L.D., and Harada, M. (2005). Development of functional human blood and immune systems in NOD/SCID/IL2 receptor gamma chain(null) mice. Blood *106*, 1565–1573.

Ito, M., Kobayashi, K., and Nakahata, T. (2008). NOD/Shi-scid IL2rgamma(null) (NOG) mice more appropriate for humanized mouse models. Curr. Top. Microbiol. Immunol. *324*, 53–76.

Izsvák, Z., Fröhlich, J., Grabundzija, I., Shirley, J.R., Powell, H.M., Chapman, K.M., Ivics, Z., and Hamra, F.K. (2010). Generating knockout rats by transposon mutagenesis in spermatogonial stem cells. Nat. Methods *7*, 443–445.

Jhappan, C., Morse, H.C., 3rd, Fleischmann, R.D., Gottesman, M.M., and Merlino, G. (1997). DNA-PKcs: a T-cell tumour suppressor encoded at the mouse scid locus. Nat. Genet. *17*, 483–486.

Katoh, M., Tateno, C., Yoshizato, K., and Yokoi, T. (2008). Chimeric mice with humanized liver. Toxicology *246*, 9–17.

Kneteman, N.M., and Mercer, D.F. (2005). Mice with chimeric human livers: who says supermodels have to be tall? Hepatology *41*, 703–706.

Kobayashi, J., Kato, A., Ota, Y., Ohba, R., and Komatsu, K. (2010). Bisbenzamidine derivative, pentamidine represses DNA damage response through inhibition of histone H2A acetylation. Mol. Cancer *9*, 34.

Leonard, W.J. (2001). Cytokines and immunodeficiency diseases. Nat. Rev. Immunol. *1*, 200–208.

Mahaney, B.L., Meek, K., and Lees-Miller, S.P. (2009). Repair of ionizing radiation-induced DNA double-strand breaks by non-homologous end-joining. Biochem. J. *417*, 639–650.

Mashimo, T., Yanagihara, K., Tokuda, S., Voigt, B., Takizawa, A., Nakajima, R., Kato, M., Hirabayashi, M., Kuramoto, T., and Serikawa, T. (2008). An ENU-induced mutant archive for gene targeting in rats. Nat. Genet. *40*, 514–515.

Mashimo, T., Takizawa, A., Voigt, B., Yoshimi, K., Hiai, H., Kuramoto, T., and Serikawa, T. (2010). Generation of knockout rats with X-linked severe combined immunodeficiency (X-SCID) using zinc-finger nucleases. PLoS ONE *5*, e8870.

McCune, J.M., Kaneshima, H., Lieberman, M., Weissman, I.L., and Namikawa, R. (1989). The scid-hu mouse: current status and potential applications. Curr. Top. Microbiol. Immunol. *152*, 183–193.

Meuleman, P., Libbrecht, L., De Vos, R., de Hemptinne, B., Gevaert, K., Vandekerckhove, J., Roskams, T., and Leroux-Roels, G. (2005). Morphological and biochemical characterization of a human liver in a uPA-SCID mouse chimera. Hepatology *41*, 847–856.

Nakamura, H., Fukami, H., Hayashi, Y., Kiyono, T., Nakatsugawa, S., Hamaguchi, M., and Ishizaki, K. (2002). Establishment of immortal normal and ataxia telangiectasia fibroblast cell lines by introduction of the hTERT gene. J. Radiat. Res. (Tokyo) *43*, 167–174.

O'Driscoll, M., and Jeggo, P.A. (2006). The role of double-strand break repair - insights from human genetics. Nat. Rev. Genet. *7*, 45–54.

Pearson, T., Greiner, D.L., and Shultz, L.D. (2008). Humanized SCID mouse models for biomedical research. Curr. Top. Microbiol. Immunol. *324*, 25–51.

Perryman, L.E. (2004). Molecular pathology of severe combined immunodeficiency in mice, horses, and dogs. Vet. Pathol. *41*, 95–100.

Pierce, A.J., and Jasin, M. (2005). Measuring recombination proficiency in mouse embryonic stem cells. Methods Mol. Biol. *291*, 373–384.

Quintana, E., Shackleton, M., Sabel, M.S., Fullen, D.R., Johnson, T.M., and Morrison, S.J. (2008). Efficient tumour formation by single human melanoma cells. Nature *456*, 593–598.

Ruis, B.L., Fattah, K.R., and Hendrickson, E.A. (2008). The catalytic subunit of DNA-dependent protein kinase regulates proliferation, telomere length, and genomic stability in human somatic cells. Mol. Cell. Biol. *28*, 6182–6195.

Shrivastav, M., De Haro, L.P., and Nickoloff, J.A. (2008). Regulation of DNA double-strand break repair pathway choice. Cell Res. *18*, 134–147.

Shultz, L.D., Ishikawa, F., and Greiner, D.L. (2007). Humanized mice in translational biomedical research. Nat. Rev. Immunol. *7*, 118–130.

Strom, S.C., Davila, J., and Grompe, M. (2010). Chimeric mice with humanized liver: tools for the study of drug metabolism, excretion, and toxicity. Methods Mol. Biol. *640*, 491–509.

Strowig, T., Rongvaux, A., Rathinam, C., Takizawa, H., Borsotti, C., Philbrick, W., Eynon, E.E., Manz, M.G., and Flavell, R.A. (2011). Transgenic expression of human signal regulatory protein alpha in Rag2-/-gamma(c)-/- mice improves engraftment of human hematopoietic cells in humanized mice. Proc. Natl. Acad. Sci. USA *108*, 13218–13223.

Taccioli, G.E., Amatucci, A.G., Beamish, H.J., Gell, D., Xiang, X.H., Torres Arzayus, M.I., Priestley, A., Jackson, S.P., Marshak Rothstein, A., Jeggo, P.A., and Herrera, V.L. (1998). Targeted disruption of the catalytic subunit of the DNA-PK gene in mice confers severe combined immunodeficiency and radiosensitivity. Immunity *9*, 355–366.

Takahashi, K., Tanabe, K., Ohnuki, M., Narita, M., Ichisaka, T., Tomoda, K., and Yamanaka, S. (2007). Induction of pluripotent stem cells from adult human fibroblasts by defined factors. Cell *131*, 861–872.

Takenaka, K., Prasolava, T.K., Wang, J.C., Mortin-Toth, S.M., Khalouei, S., Gan, O.I., Dick, J.E., and Danska, J.S. (2007). Polymorphism in Sirpa modulates engraftment of human hematopoietic stem cells. Nat. Immunol. *8*, 1313–1323.

Tateno, C., Yoshizane, Y., Saito, N., Kataoka, M., Utoh, R., Yamasaki, C., Tachibana, A., Soeno, Y., Asahina, K., Hino, H., et al. (2004). Near completely humanized liver in mice shows human-type metabolic responses to drugs. Am. J. Pathol. *165*, 901–912.

Tesson, L., Usal, C., Ménoret, S., Leung, E., Niles, B.J., Remy, S., Santiago, Y., Vincent, A.I., Meng, X., Zhang, L., et al. (2011). Knockout rats generated by embryo microinjection of TALENs. Nat. Biotechnol. *29*, 695–696.

Tong, C., Li, P., Wu, N.L., Yan, Y., and Ying, Q.L. (2010). Production of p53 gene knockout rats by homologous recombination in embryonic stem cells. Nature *467*, 211–213.

van der Burg, M., Ijspeert, H., Verkaik, N.S., Turul, T., Wiegant, W.W., Morotomi-Yano, K., Mari, P.O., Tezcan, I., Chen, D.J., Zdzienicka, M.Z., et al. (2009). A DNA-PKcs mutation in a radiosensitive T-B- SCID patient inhibits Artemis activation and nonhomologous end-joining. J. Clin. Invest. *119*, 91–98.

Wege, A.K., Melkus, M.W., Denton, P.W., Estes, J.D., and Garcia, J.V. (2008). Functional and phenotypic characterization of the humanized BLT mouse model. Curr. Top. Microbiol. Immunol. *324*, 149–165.

Yamasaki, C., Kataoka, M., Kato, Y., Kakuni, M., Usuda, S., Ohzone, Y., Matsuda, S., Adachi, Y., Ninomiya, S., Itamoto, T., et al. (2010). In vitro evaluation of cytochrome P450 and glucuronidation activities in hepatocytes isolated from liver-humanized mice. Drug Metab. Pharmacokinet. *25*, 539–550.

Yan, C.T., Boboila, C., Souza, E.K., Franco, S., Hickernell, T.R., Murphy, M., Gumaste, S., Geyer, M., Zarrin, A.A., Manis, J.P., et al. (2007). IgH class switching and translocations use a robust non-classical end-joining pathway. Nature *449*, 478–482.

Zha, S., Jiang, W., Fujiwara, Y., Patel, H., Goff, P.H., Brush, J.W., Dubois, R.L., and Alt, F.W. (2011). Ataxia telangiectasia-mutated protein and DNA-dependent protein kinase have complementary V(D)J recombination functions. Proc. Natl. Acad. Sci. USA *108*, 2028–2033.

BRAIN RESEARCH 1435 (2012) 154–166

Available online at www.sciencedirect.com

SciVerse ScienceDirect

www.elsevier.com/locate/brainres

BRAIN RESEARCH

Research Report

Kcna1-mutant rats dominantly display myokymia, neuromyotonia and spontaneous epileptic seizures

Saeko Ishida[a], *Yu Sakamoto*[b], *Takeshi Nishio*[c], *Stéphanie Baulac*[a,d,e], *Mitsuru Kuwamura*[f], *Yukihiro Ohno*[g], *Akiko Takizawa*[a], *Shuji Kaneko*[b], *Tadao Serikawa*[a], *Tomoji Mashimo*[a,*]

[a]*Institute of Laboratory animals, Graduate School of Medicine, Kyoto University, Kyoto 606-8501, Japan*
[b]*Department of Molecular Pharmacology, Graduate School of Pharmaceutical Sciences, Kyoto University, Kyoto 606-8501, Japan*
[c]*Department of Integrative Brain Science, Graduate School of Medicine, Kyoto University, Kyoto 606-8501, Japan*
[d]*Inserm U975, CRICM, Paris F-75013, France*
[e]*Université Pierre & Marie Curie-Paris 6, UMR_S975, Paris F-75013, France*
[f]*Laboratory of Veterinary Pathology, Osaka Prefecture University, Izumisano, Osaka 598-8531, Japan*
[g]*Laboratory of Pharmacology, Osaka University of Pharmaceutical Sciences, Takatsuki 569-1094, Japan*

ARTICLE INFO

Article history:
Accepted 8 November 2011
Available online 13 November 2011

Keywords:
Episodic ataxia type 1 (EA1)
Animal model
Phenotype-driven ENU mutagenesis
Voltage-gated potassium channel shaker-related subfamily member 1 (Kcna1)
Voltage-sensor domain S4
Dominant-negative effect

ABSTRACT

Mutations in the KCNA1 gene, which encodes for the α subunit of the voltage-gated potassium channel Kv1.1, cause episodic ataxia type 1 (EA1). EA1 is a dominant human neurological disorder characterized by variable phenotypes of brief episodes of ataxia, myokymia, neuromyotonia, and associated epilepsy. Animal models for EA1 include *Kcna1*-deficient mice, which recessively display severe seizures and die prematurely, and V408A-knock-in mice, which dominantly exhibit stress-induced loss of motor coordination. In the present study, we have identified an N-ethyl-N-nitrosourea-mutagenized rat, named autosomal dominant myokymia and seizures (ADMS), with a missense mutation (S309T) in the voltage-sensor domain, S4, of the *Kcna1* gene. ADMS rats dominantly exhibited myokymia, neuromyotonia and generalized tonic–clonic seizures. They also showed cold stress-induced tremor, neuromyotonia, and motor incoordination. Expression studies of homomeric and heteromeric Kv1.1 channels in HEK cells and *Xenopus* oocytes, showed that, although S309T channels are transferred to the cell membrane surface, they remained non-functional in terms of their biophysical properties, suggesting a dominant-negative effect of the S309T mutation on potassium channel function. ADMS rats provide a new model, distinct from previously reported mouse models, for studying the diverse functions of Kv1.1 in vivo, as well as for understanding the pathology of EA1.

1. Introduction

Episodic ataxia type 1 (EA1) is an autosomal dominant neurological disorder, with an age of onset in childhood or early adolescence. EA1 is characterized by myokymia (involuntary quivering or rippling of muscle bundles), and episodic attacks of ataxia (loss of motor coordination and balance with spastic contractions of the skeletal muscles) (Pessia and Hanna, 1993;

* *Corresponding author at:* Institute of Laboratory Animals, Graduate School of Medicine, Kyoto University, Yoshidakonoe-cho, Sakyo-ku, Kyoto 606-8501, Japan. Fax: +81 75 753 4409.
E-mail address: tmashimo@anim.med.kyoto-u.ac.jp (T. Mashimo).

0006-8993/$ – see front matter © 2011 Elsevier B.V. All rights reserved.
doi:10.1016/j.brainres.2011.11.023

Rajakulendran et al., 2007). EA1 is also associated with an increased incidence of epilepsy (Zuberi et al., 1999) and hypomagnesaemia (Glaudemans et al., 2009a). Since clinical manifestations of EA1 are widely variable, with respect to the severity of ataxia and myokymia, and the occurrence of neuromyotonia (muscle stiffness, twitching, and fasciculation), and epilepsy (Eunson et al., 2000; Gilbert et al., 2011; Poujois et al., 2006; Tomlinson et al., 2010), clinical diagnosis is based on genetic testing of *KCNA1*. *KCNA1* encodes the α subunit of the voltage-gated potassium channel, Kv1.1, and is the only known gene associated with EA1 (Browne et al., 1994). The *KCNA1* mutations reported in EA1 patients are predominantly missense mutations that are distributed throughout the gene. However, a nonsense mutation has also been identified at the C-terminal end of *KCNA1* (Eunson et al., 2000). The phenotypic variability of EA1 may be associated with the distinct mutations of *KCNA1*; however, phenotypic differences are present not only among families, but also among individuals carrying the same mutation within the same family, suggesting the interplay of modifier genes and/or non-genetic factors (Gilbert et al., 2011). Because of this high degree of intra- and interfamilial genetic and environmental variability, determining genotype–phenotype correlations in humans is problematic. Animal models can greatly improve our understanding of human disease pathogenesis under the control of specific genetic and environmental conditions.

N-ethyl-N-nitrosourea (ENU) mutagenesis has been widely used to generate animal models of human diseases by two complementary approaches, forward and reverse genetics. A reverse genetics, or gene-driven approach (gene to phenotype), screens for mutations within a gene of interest, in ENU-mutagenized animals, enabling subsequent investigation of gene function. For the reverse genetics approach, we have generated a large repository of ENU-mutagenized rats, the Kyoto University Rat Mutant Archive (KURMA: http://www.anim.med.kyoto-u.ac.jp/enu) (Mashimo et al., 2008). KURMA contains genomic DNA and frozen sperm from 10,000 ENU-mutagenized G1 rats, and will be used to screen mutations of targeted genes using a high-throughput screening assay based on the Mu-transposition reaction (MuT-POWER). Subsequent recovery of corresponding sperm by intracytoplasmic sperm injection (ICSI), will establish gene-targeted rat models of human diseases (Mashimo et al., 2010; Yoshimi et al., 2009). Alternatively, a forward genetics, or phenotype-driven approach (phenotype to gene), involves screening ENU-mutagenized animals for abnormal phenotypes, and then mapping the casual mutation. The forward genetic approach allows mutagenized animals expressing symptoms of interest to be identified, and may offer new insight into disease pathogenesis.

In this study, we used a forward genetic screen on ENU-mutagenized G1 rats to identify neurological phenotypes. We identified a rat exhibiting persistent myokymia, neuromyotonia, and spontaneous epileptic seizures, subsequently named autosomal-dominant myokymia and seizures (ADMS) rats. Positional cloning identified a missense mutation (S309T), in the *Kcna1* gene, located in the voltage-sensor segment (S4), of Kv1.1. The S309T mutation is in close proximity to the L305F mutation previously identified in a French EA1 family, exhibiting brief episodes of ataxia in early childhood and progressive development of chronic neuromyotonia (Poujois et al., 2006). Thus ADMS rats provide a new model of EA1, which are genetically and phenotypically different from previously reported mouse models.

2. Results

2.1. *An ENU-mutagenized rat exhibiting twitching and spontaneous seizures*

In the first generation of the progeny (G1) from an ENU-injected F344 male, one female exhibited abnormal behaviours, characterized by muscle twitching and spontaneous convulsive seizures. To determine the mode of inheritance, this "affected" G1 female was backcrossed with an F344 male. Of the backcross progeny, 16 (53.3%) rats exhibited the abnormal behaviours, with 14 (46.7%) rats phenotypically normal. Both twitching and seizure behaviours always co-segregated, and there were no gender differences. Further backcrossing of affected males to F344 females, for ten generations (N10), resulted in approximately 50% of the progeny affected and 50% unaffected in each generation. This pattern of inheritance, suggests that on an F344 genetic background, the abnormal behaviours of muscle twitching and seizures, are inherited in an autosomal dominant pattern. Thus, we named this inbred strain of rats, autosomal-dominant myokymia and seizures (ADMS).

Interestingly, compared with F344 rats, ADMS rats showed slightly but significantly increased body weight from 10 to 13 weeks of age (Fig. 1A), that coincided with severe twitching behaviour. Physically, the ADMS rats appeared swollen, and were not obese. From 16 weeks of age, the body weight of ADMS rats significantly decreased, compared with F344 rats, coinciding with severe periodic seizures. By 30 weeks of age, 84% of ADMS rats had died. In contrast, no F344 or ADMS rats on a BN background, died at this age (Fig. 1B). This increased mortality in ADMS rats coincided with a reduced body weight and increased number of convulsive seizures. Postmortem examination showed no obvious morphological abnormalities in any tissues examined from ADMS rats.

2.2. *Neuromyotonia and myokymia in ADMS rats*

ADMS rats began to display muscle twitching from 6 weeks of age, typically characterized by coordinated muscle contraction of the eyelid, the neck, and the extremities (Fig. 1C; Supplementary Video 1). Startle responses, twitching behaviour in response to sudden acoustic stimuli such as clapping hands, was also evident (Fig. 1D). The number of twitches increased with age until 18 weeks, then decreased, coinciding with loss of mobility, reduced body weight and increased convulsive seizures in the rats. To further characterize muscle twitching in ADMS rats, we used EMG to record muscle activity from fore and hind limbs (Fig. 1D). Spontaneous myoclonic discharges, correlating with muscle twitching, were detected from the hind limbs. Large spikes were recorded from both fore and hind limbs in response to sound stimulation, reflecting myoclonic startle responses. Importantly, EMG recordings from fore limbs

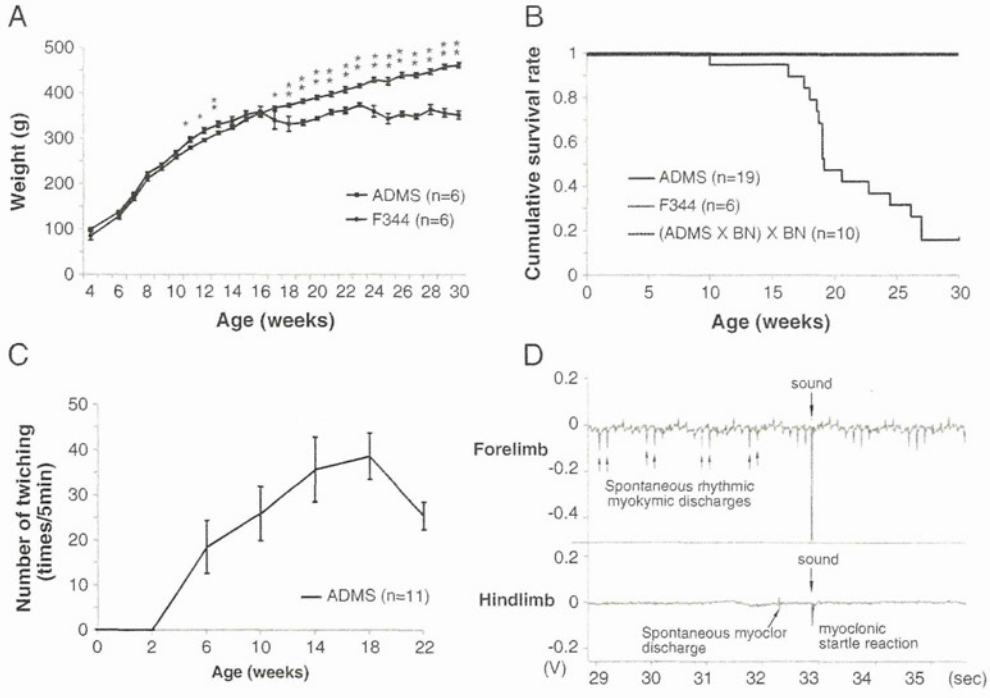

Fig. 1 – Gross and myokymic phenotypes in ADMS rats. (A) Comparison of body weight between ADMS (n=6) and F344 (n=6) rats. ADMS rats show increased body weight from 10 weeks of age, which is then reduced, in conjunction with the severe convulsive seizures from 18 weeks of age. Error bars indicate SEM. Unpaired student's t-test: *p<0.05, **p<0.01. (B) Kaplan–Meier survival curves of ADMS (n=19), F344 (n=6) rats, and (ADMS×BN)×BN backcross progeny (n=10). By 30 weeks of age, 84% of ADMS rats had died. (C) Twitching behaviours appeared from 6 weeks of age and peaked at 18 weeks of age in ADMS rats (n=11). Error bars indicate SEM. (D) Electromyogram (EMG) recording of forelimb and hindlimb muscles during the interictal period in 16-week-old ADMS rats. A spontaneous myoclonic discharge was detected from the hindlimb, as well as a myoclonic startle reaction in response to a sound stimulus. Spontaneous rhythmic myokymic discharges (7 Hz) were detected from the forelimb.

also showed rhythmic multiple discharges with an intraburst frequency of 7 Hz. This firing pattern is similar to that observed in human myokymia.

2.3. *Spontaneous convulsive seizures in ADMS rats*

ADMS rats exhibited spontaneous convulsive seizures from 10 weeks of age (Fig. 2A). Occurrence of seizures was aggravated during cage changing or animal handling. Seizure onset was observed in all ADMS rats (n=11) by 16 weeks of age. The average number of seizures significantly increased with age until 20 weeks of age (Fig. 2A), while the mean duration of each seizure did not increase (Fig. 2B). The typical seizure phenotype encompassed four stages: (i) initial sudden falling down, (ii) secondly jerking of the entire body or the extremities as clonic phase, occasionally with a tonic phase with stiffening of the entire body, (iii) immobility, and (iv) rearing with muscle twitching (Fig. 2C; Supplementary Video 2). Motor automatisms, such as repetitive chewing, occasionally occurred during the seizure. Cortical and hippocampal EEG recordings identified four characteristic EEG patterns corresponding to the four stages of the seizure phenotype. First, aberrant large spike activity associated with falling-down behaviour (i). Second, low-voltage fast wave discharges detected during the tonic stage, and spike-and-wave discharges (2 Hz) detected during the clonic convulsive stage (ii). These discharges terminated abruptly, followed by fast spikes with low to high voltages in the freezing stage (iii). Finally, polyspike and large wave complexes (1–3 Hz) during the rearing stage (iv). Although cortical and hippocampal EEG recordings were generally synchronized, ictal epileptic activities in the hippocampus tended to precede cortical discharges, specifically at the onset of seizure ((i) initial sudden falling), and/or during the transition stage between freezing (iii) and rearing (iv). The behavioural phenotypes and abnormal discharge patterns in ADMS rats are similar to other rodent models of temporal lobe epilepsy (Rho et al., 1999; Wenzel et al., 2007). These spontaneous convulsive seizures and the twitching phenotypes were significantly prevented 30 min after the administration of carbamazepine (CBZ) in ADMS rats (n=5) (Figs. 2D, E). Histopathological analysis of ADMS rats at 16–19 weeks of age revealed no major abnormalities in haematoxylin staining of the brain (Supplementary Fig. 1).

2.4. *Identification of a Kcna1 S309T mutation*

We crossed ADMS females to BN males, a rat strain suitable for genetic mapping studies, because of their distinct genetic background. We obtained eight F1 progeny exhibiting the

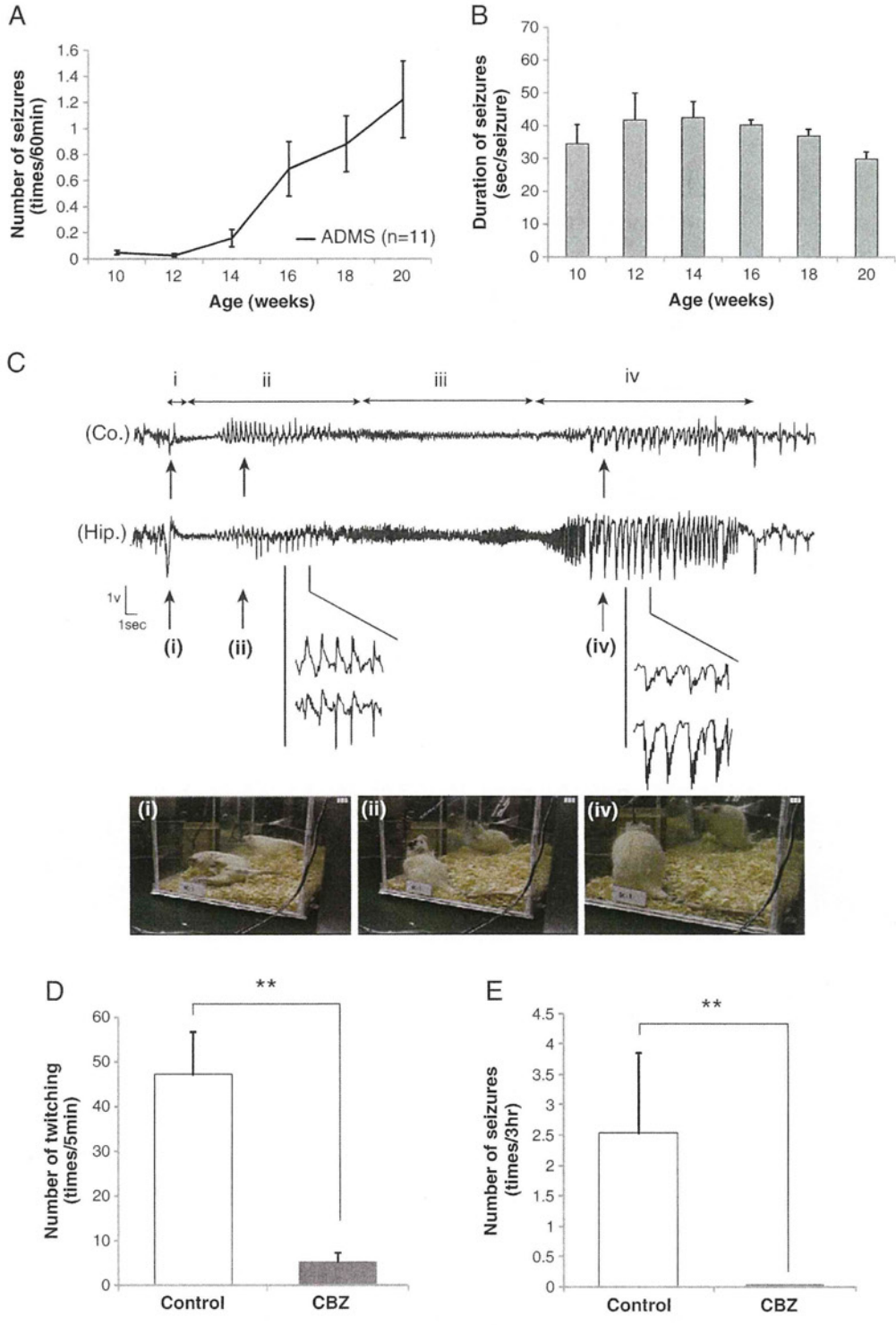

Fig. 2 – Spontaneous epileptic seizures in ADMS rats. (A) Convulsive seizures started from 10 weeks of age and increased in number, peaking at 20 weeks of age in ADMS rats (n = 11). Error bars indicate SEM. (B) The mean duration of seizures did not differ between ages. Unpaired student's *t*-test: $p > 0.05$. (C) Cortical (Co.) and hippocampal (Hip.) electroencephalogram (EEG) recorded from an ADMS rat at 16 weeks of age. Although the discharges occurred synchronously in both cortex and hippocampus, the amplitude was higher in hippocampus than in cortex. Behavioural patterns were correlated with EEG events. i: tonic attack; ii: clonus of the limbs; iii: immobility; and iv: rearing with chewing gesture. Photographs show characteristic postures in stages i, ii and iv. (D) The spontaneous convulsive seizures in ADMS rats (n = 5) were prevented by the administration of carbamazepine (CBZ). (E) Numbers of the twitching behaviours in ADMS rats (n = 5) were significantly decreased by CBZ. Paired student's *t*-test: $^{**}p < 0.01$.

same abnormal behaviours as the ADMS rats, albeit with a slightly delayed onset. Muscle twitching was observed from 10 to 12 weeks of age, compared with 6 weeks in ADMS rats, while spontaneous convulsive seizures were not evident until 20–30 weeks of age in four animals, with the remaining four animals not presenting with seizures until 40 weeks, suggesting modifier gene(s) are associated with the onset of seizures. Further breeding, generated 180 (ADMS×BN)×BN

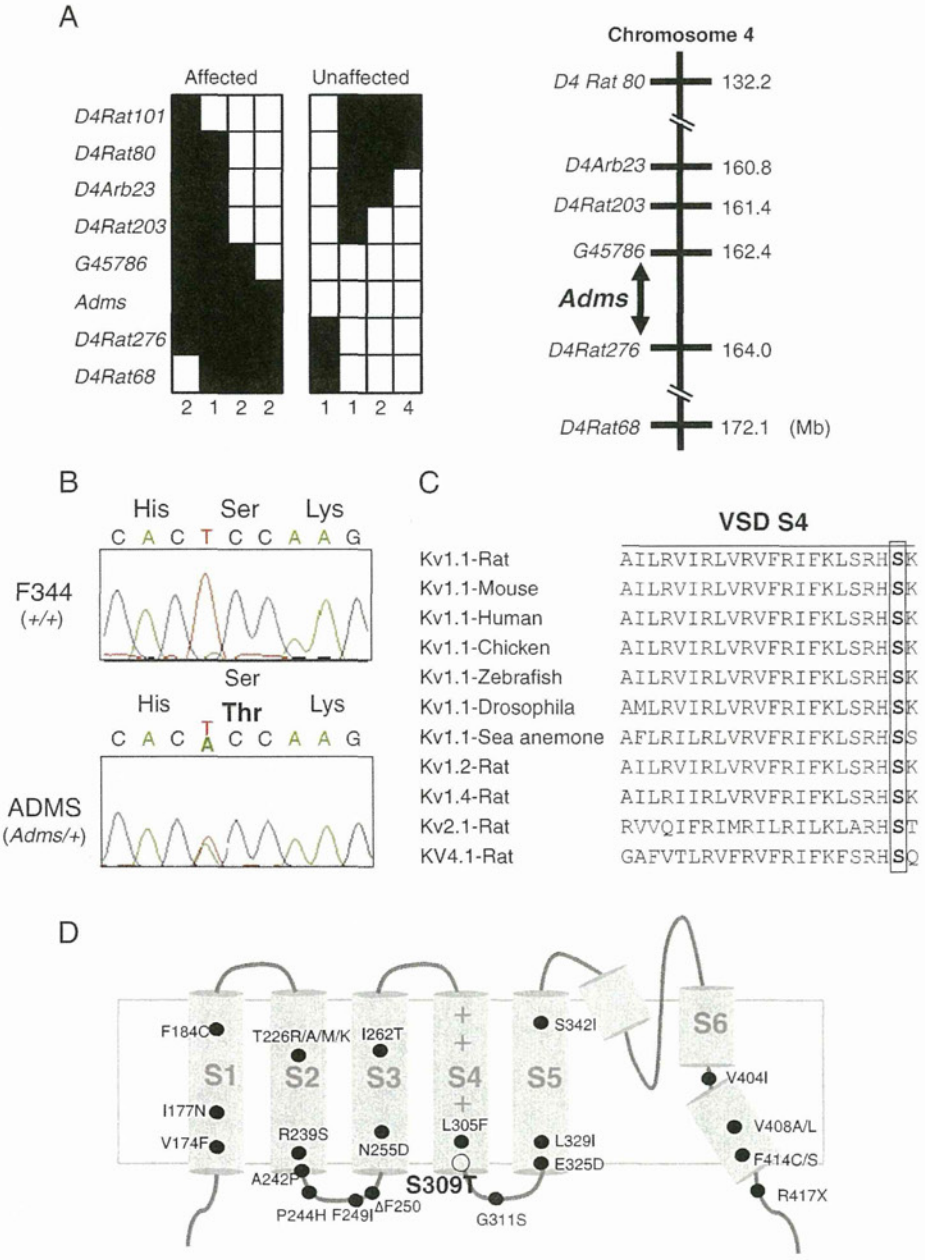

Fig. 3 – Identification of *Adms* mutation. (A) (Left) Distribution of haplotypes in (ADMS×BN)×BN backcross progeny, determined using SSLP markers from rat chromosome 4. White boxes represent BN homozygous alleles or 'unaffected' for *Adms*. Black boxes represent F344-derived heterozygotes or 'affected' alleles. Numbers of the backcross progeny are depicted at the bottom of the haplotypes. (Right) *Adms* was mapped to a 1.6-Mb region between *G45786* and *D4Rat276*. (B) Sequencing analysis in F344 (upper) and ADMS (lower) rats revealed a nucleotide change from T to A (arrowhead) located at position 925 of the *Kcna1* gene. The mutation results in an amino acid substitution of serine (Ser) with threonine (Thr) at codon 309 of the KCNA1 protein. (C) Amino acid sequence alignment of the voltage-sensor domain S4 of KCNA1 in several species and between KCNA families. The S309T amino acid substitution (boxed) is located in a region highly conserved among species and within the KCNA family. (D) Schematic representation of the Kv1.1 subunit. Black circles represent the positions of the EA1 mutations thus far reported and a white circle represents the rat *Adms* mutation.

backcross progeny, with 87 rats expressing the twitching phenotype at 10–14 weeks of age, and seizure activity from 20 weeks of age.

Genome-wide scanning using 121 SSLP markers mapped the *Adms* locus to a 1.6-Mb genomic region, between markers G45786 and D4Rat276 on Chr 4 (Fig. 3A). Eighteen known or predicted genes within the *Adms* region were obtained from the Ensembl database (http://www.ensembl.org). Among them were the voltage-gated potassium channel families, *Kcna1*, *Kcna5*, and *Kcna6*, that we deemed to be good candidates, based on their functional ability to regulate membrane potential, neuronal excitability, and nerve signalling (Johnston et al., 2010; Wulff et al., 2009). In particular, the behavioural phenotypes of ADMS rats were similar to those of *Kcna1*-deficient mice (Smart et al., 1998), and to the symptoms reported in human EA1 (Pessia and Hanna, 1993; Rajakulendran et al., 2007). We compared the sequences of *Kcna1*, *Kcna5*, and *Kcna6* between F344 and ADMS rats, and identified a T-to-A mutation at nucleotide 925 of the *Kcna1* gene, but no mutations in *Kcna5* and *Kcna6* genes (Fig. 3B). The T925A mutation of *Kcna1* results in a substitution of serine for threonine at residue 309, which is located in the voltage sensor segment, S4, of Kv1.1. This residue is highly conserved among species and other potassium channel family genes (Fig. 3C). To date, more than 20 *KCNA1* mutations have been reported in EA1 patients (Bretschneider et al., 1999; Browne et al., 1994; Browne et al., 1995; Chen et al., 2007; Comu et al., 1996; Demos et al., 2009; Eunson et al., 2000; Glaudemans et al., 2009b; Graves et al., 2010; Imbrici et al., 2008; Kinali et al., 2004; Klein et al., 2004; Knight et al., 2000; Lee et al., 2004; Poujois et al., 2006; Scheffer et al., 1998; Shook et al., 2008; Zerr et al., 1998; Zuberi et al., 1999) (Fig. 3D). Interestingly, the *KCNA1* missense mutation L305F, which is closely located to S309T in the S4 segment, was reported in an EA1 family uniquely exhibiting brief episodes of cerebellar ataxia in early childhood and progressive development of chronic neuromyotonia with muscle rippling and hypertrophy (Poujois et al., 2006).

2.5. *Premature death of homozygous S309T rats*

To investigate the effect of the homozygous mutation of *Kcna1* S309T, we crossed N10 heterozygous ADMS males and females. The behaviour and appearance of homozygous *S309T/S309T* rats at birth did not differ from those of heterozygous S309T/+ and WT+/+ littermates. Western blot analysis showed that the expression level of endogenous KCNA1 protein in the brain did not differ between homozygous, heterozygous and WT littermate rats (Supplementary Fig. 2). However, from postnatal day 14, development of the homozygous rats was dramatically impaired and body weight significantly decreased compared with heterozygous and WT littermates (Fig. 4A). In conjunction with reduced body weight, the homozygous rats showed tremors, motor incoordination, mainly caused by extension of hind limbs, and spontaneous convulsive seizures (Supplementary Video 3). These phenotypes progressively worsen with age. Homozygous pups became inactive except during seizures, and usually remained isolated from their mother. All homozygous rats died prematurely with a mean lifetime of 16 days (Fig. 4B).

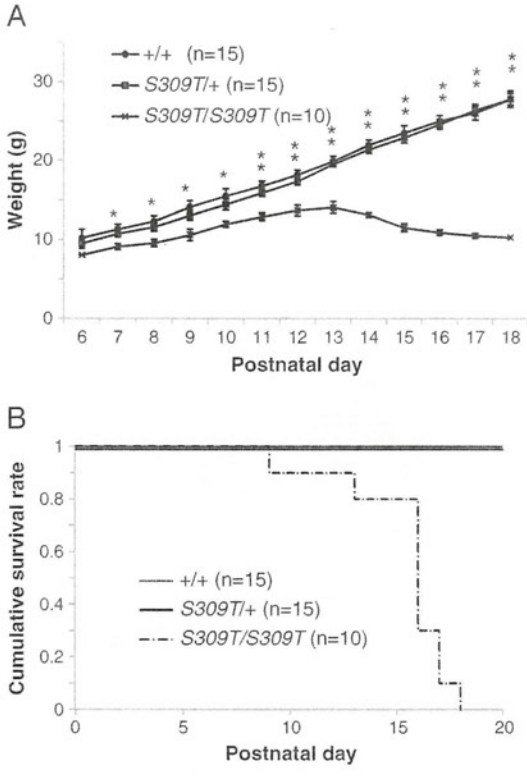

Fig. 4 – Lethality of homozygous S309T rats. (A) From postnatal (P) 7 days, the body weight of homozygous S309T/S309T rats (n = 10) was significantly reduced compared with heterozygous S309T/+ (n = 15) and WT+/+ (n = 15) rats. Error bars indicate SEM. Unpaired student's t-test: *p < 0.05, **p < 0.01. (B) Kaplan–Meier survival curves of homozygous S309T/S309T (n = 10), heterozygous S309T/+ (n = 15) and WT+/+ (n = 15) rats. All homozygous rats had died by P18.

No homozygous rats survived beyond postnatal day 18, while neither heterozygous or WT littermates died at this age. Postmortem examination of homozygous rats detected an absence of stomach contents, suggesting early mortality might result from feeding failure partially caused by the severe behavioural phenotypes.

2.6. *Motor incoordination by cold-swim tests*

To examine whether ADMS rats show cold-swim induced neuromyotonia and motor incoordination that were recognized in *Kcna1*-deficient mice (Zhou et al., 1998), we forced rats to swim in a tank filled with either warm (38 °C) or cold (17 °C) water. We used 5-week-old ADMS rats that have never exhibited muscle twitching or spontaneous seizures. In warm water, there was no behavioural difference between ADMS and WT rats during 2-min swimming in the tank and subsequent 5-min observation on a dry platform at room temperature. In cold water however, there was an observable difference between ADMS and WT rats. Toward the end of the 2-min swimming period, ADMS rats had difficulties maintaining axial orientation and

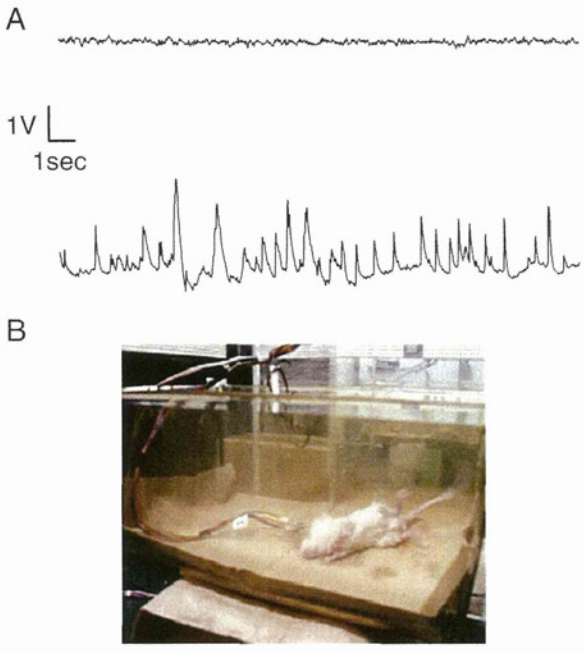

Fig. 5 – Cortical EEG recording in ADMS rat by cold-swim tests. (A) EEG recorded from an ADMS rat before the test (upper) and during the cold-swim induced clonus behaviour (lower). (B) A photograph shows characteristic posture during the clonus behaviour.

swimming, showing head shaking and twitching behaviour in the water. When removed from the water, ADMS rats exhibited severe neuromyotonia (Supplementary Video 4) and tremors, with the eyes shut and whiskers flickering. After a few minutes of tremors lasting, and even worsening, the rats demonstrated head nodding, forelimb clonus and rearing. Cortical EEG recordings showed aberrant spike-and-wave discharges (2-3 Hz) associated with clonus behaviours (Figs. 5A, B). The tremors and clonus phenotypes were reduced as time progressed, but when the animals started to walk, its movements were staggering and ataxic (Supplementary Video 5). Normal behaviour was fully recovered after 20 min. Cold-swim induced tremors, neuromyotonia, clonus, and motor incoordination, were present in all ADMS rats tested (n=7). In contrast, none of the behaviours was observed in WT rats (n=5).

2.7. *Electrophysiological properties of S309T channel*

To investigate the functional consequences of the S309T mutation on the Kv1.1 channel, we transfected HEK 293 cells with *Kcna1* cDNA (WT or S309T) and recorded whole-cell current responses. At a holding potential of −80 mV, current families were obtained by sequential 100-ms depolarizing commands from −100 to 50 mV, delivered in 10 mV increments. Typical delayed-rectifier potassium currents were recorded from cells expressing Kv1.1 WT, whereas minimal currents were detected from cells expressing Kv1.1 S309T or from mock-transfected cells (Figs. 6A, B). In western blot analysis, a single 56-kD band was detected in cells transfected with *Kcna1* WT or S309T cDNA (Fig. 6C). To investigate whether the S309T mutation has an effect on the intracellular trafficking of Kv1.1, we analysed the cell-surface expression of Kv1.1, by biotinylating the surface proteins on HEK cells. Precipitation of the solubilized biotinylated proteins with streptavidin beads, followed by western blotting, detected expression of both WT and S309T variants of Kv1.1 on the cell surface (Fig. 6D).

Because ADMS rats carrying the *Kcna1* S309T mutation dominantly display several neurological abnormalities, the opening of Kv1.1 channels may be disturbed when one or more S309T-containing subunits are incorporated into the tetrameric complex of Kv1.1 channels. To test this hypothesis, we co-injected cRNAs for WT and S309T mutant subunits in *Xenopus* oocytes, and measured current responses under a two electrode voltage clamp configuration. At a holding potential of −60 mV, current families were obtained by 500-ms depolarizing commands (with a 500 ms prepulse at −120 mV) from −60 to 60 mV, delivered in 20 mV increments. The co-injection of WT and S309T cRNA (1:1 ratio) resulted in reduced outward currents, with an approximately 80% smaller amplitude than that of WT-injected oocytes at 0 mV, suggesting a dominant-negative effect of the S309T subunit on the function of heterotetrameric Kv1.1 channels (Figs. 6E, F). Western blot analysis showed equivalent Kv1.1 protein expression levels among the three groups (WT, S309T and WT:S309T (1:1) co-injected) of oocytes (Fig. 6G).

3. Discussion

Table 1 summarizes the *Kcna1*-mutant animal models for EA1 previously reported in mice and rats. They exhibit diverse neurological phenotypes and show differing functional defects of the potassium channel, Kv1.1 (Herson et al., 2003; Petersson et al., 2003; Smart et al., 1998). *Kcna1*-knockout mice have a complete deletion of *Kcna1*, and have enormously contributed to our fundamental understanding of Kv1.1 function (Glasscock et al., 2010; Kopp-Scheinpflug et al., 2003; Lopantsev et al., 2003; Smart et al., 1998; Zhang et al., 1999; Zhou et al., 1998). Homozygous *Kcna1*-knockout mice exhibit various neurological defects, namely, spontaneous seizure activities associated with elevated excitability of the hippocampal CA3 neurons (Lopantsev et al., 2003), and/or of the auditory neurons of the medial nucleus of the trapezoid body (MNTB) (Kopp-Scheinpflug et al., 2003). Other defects include temperature-sensitive nerve excitability in the PNS (Zhou et al., 1998), alteration of GABAergic inhibition in cerebellar Purkinje cells (Zhang et al., 1999), and premature death potentially associated with cardiac dysfunction (Glasscock et al., 2010). However, to date, no mutation causing a complete deletion of the *KCNA1* gene has been reported in human EA1. Spontaneous mutant mice, *megencephaly*, expressing a truncated KCNA1 protein of 230 residues, recessively exhibit progressive brain overgrowth and epileptic behaviours similar to knockout mice (Persson et al., 2005; Petersson et al., 2003). *Kcna1*-knockin mice induced by the V408A EA1 mutation, show stress-induced loss of motor coordination, which mimics the symptoms of human EA1 (Herson et al., 2003). However, none of the mouse models shows spontaneous behavioural

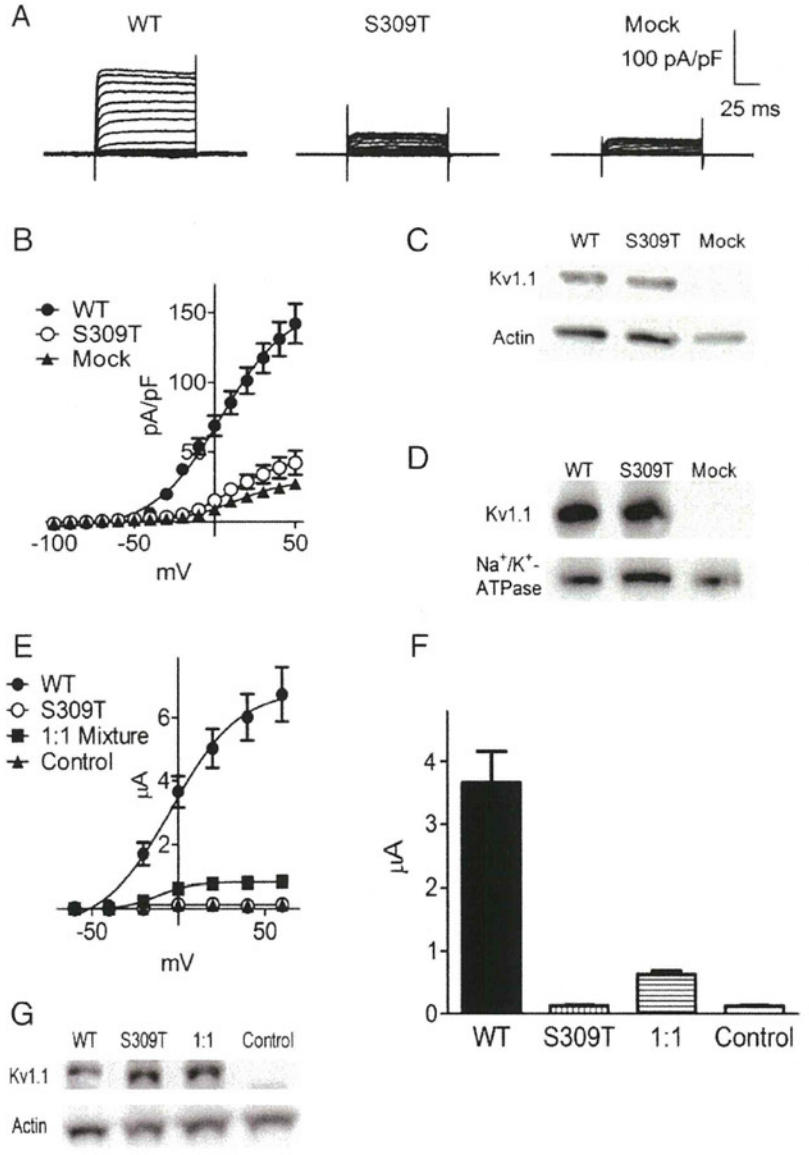

Fig. 6 – Electrophysiological properties of S309T channel. (A) Typical whole-cell current families recorded from HEK 293 cells transfected with cDNAs encoding Kv1.1 WT (left), S309T (centre) and transfection control (mock, right). Minimal currents were detected from cells expressing Kv1.1 S309T or from mock-transfected cells. (B) I–V relationships of Kv1.1 channels recorded from HEK cells transfected with each variant (n = 4–5). (C, D) Western blot analysis of (C) whole cell lysate and (D) cell surface fractions of HEK cells transfected with each variant. Both WT and S309T Kv1.1 proteins were expressed on the cell surface. (E) I–V relationships of Kv1.1 channels recorded from *Xenopus* oocytes injected with WT cRNA, S309T cRNA and 1:1 mixture of WT and S309T cRNAs (n = 4). The total amount of injected cRNAs was adjusted to 5 ng/oocyte. (F) Current amplitude recorded in response to 0 mV voltage pulse shown in (E). The co-injection of WT and S309T cRNA resulted in 80% smaller currents than WT-injected oocytes. (G) Western blot analysis indicated equivalent Kv1.1 protein expression levels among the three groups of cRNA injected oocytes, WT, S309T and WT:S309T (1:1) co-injected.

phenotypes in heterozygotes, in contrast to the ADMS rats, which we have shown to dominantly express convulsive seizures, myokymia and neuromyotonia. These neurological phenotypes are similar to symptoms of human EA1, and are severe compared with current mouse models. Interestingly, as far as we know, the myokymia phenotype detected by EMG recording in ADMS rats, has not been reported in any of the mouse models, but is always detected in individuals with human EA1. Considering EA1 patients exhibiting myokymia in the limbs or especially in the muscles of the face or the hands (Pessia and Hanna, 1993), myokymia with a predilection for forelimbs of ADMS rats may partially mimic the EA1 symptoms of human patients.

What mechanism is responsible for the phenotypic differences between the EA1 models? Strain-dependent genetic

Table 1 – Phenotype comparison of *Kcna1* mutant animals and relevance as EA1 models.

Animals	Mutation		Phenotypes				Protein functions in vitro		
			Lethality	Seizure (CNS)	Myokymia, neuromyotonia (PNS)	Episodic ataxia (cerebellum)	Channel activity	Expression, trafficking	Tetrameric channels
Kcna1 knockout mice (Smart et al., 1998)	Null	Hetero	–	± susceptible to flurothyl-induced seizures	–	–	↓↓↓ no activity	↓ half expression	–
		Homo	~50% die until 5 weeks	+++ spontaneous seizures start from 3–4 weeks	± cold-swim induced tremor and neuromyotonia	± cold-swim induced motor incoordination		↓↓↓ no expression	
megencephaly mice (Petersson et al., 2003)	Truncation at 230aa	Hetero	- (increased brain volume)	–	–	–	↓↓↓ no activity	–	Forming tetramers, impeded?
		Homo		+++ spontaneous seizures start from 5–6 weeks	+ startle responses	+ shakiness in gait		↓↓↓ trapped in endoplasmic reticulum	
V408A knockin mice (Herson et al., 2003)	Missense V408A	Hetero	–	–	–	± isoproterenol-induced motor incoordination	↓↓ reduced current, slow inactivation	Normal expression and trafficking	Interrupting WT-Kv1.1 channels
		Homo	embryonic lethal at E3-E9	–	–	–			
ADMS S309T rats	Missense S309T	Hetero	~80% die until 30 weeks	+++ spontaneous seizures start from 12–14 weeks	+++ myokymia, neuromyotonia, startle responses	± cold-swim induced motor incoordination	↓↓↓ no current	Normal expression and trafficking	Interrupting WT-Kv1.1 channels
		Homo	postnatal lethal at P10–P18	++++ spontaneous seizures start from P10	++++ extension of hind limbs, tremor	+++ ataxia			

background or species differences between mouse and rat likely play a part. Seizure onset was delayed or even prevented in F1 and BC1 progeny of BN rats, suggesting the influence of modifier gene(s). In human EA1, neuromyotonia is generally associated with KCNA1 mutations; conversely, epilepsy is not associated with mutations in potassium channels, but with other factors such as modifier genes (Pessia and Hanna, 1993; Poujois et al., 2006; Rajakulendran et al., 2007; Zuberi et al., 1999). In mice, impaired Ca^{2+}-channel function as a result of *Cacna1a* mutations, show improved seizure susceptibility by altering neuronal network excitability in *Kcna1*-knockout mice, demonstrating protective interactions between ion channel variants (Glasscock et al., 2007). A further interaction between *Kcna1* and another gene, *Lgi1*, was implicated in a rare autosomal dominant form of temporal lobe epilepsy, and shown to modulate fast inactivation of Kv1.1 (Schulte et al., 2006). Further genetic analysis focusing on seizure susceptibility in the (ADMS×BN)×BN backcross progeny may offer insights into the modifier gene(s) associated with seizure onset.

The distinct mutations of *Kcna1* may explain the wide variety of clinical phenotypes in EA1. Our expression studies of homomeric S309T Kv1.1 channels in HEK cells indicated cell-surface expression of the channels is non-functional in terms of their biophysical properties (Fig. 6). Heteromeric expression of S309T and WT Kv1.1 channels in *Xenopus* oocytes resulted in greatly reduced currents compared with WT Kv1.1 channels, suggesting the S309T mutation has a dominant-negative effect on the potassium channel, consistent with previous functional studies on EA1 mutations (Chen et al., 2007; D'Adamo et al., 1999; Imbrici et al., 2011; Zuberi et al., 1999). The *mceph* truncated protein, containing only the N-terminal domain, is retained in the endoplasmic reticulum and not expressed on the cell surface (Persson et al., 2005) (Table 1). On the other hand, V408A Kv1.1 channels show normal cell-surface expression and partially reduced potassium currents (Adelman et al., 1995). It was also reported that the V408A Kv1.1 channels reduce the rate of inactivation by a decreased affinity for the N-terminal inactivation domain of co-assembled WT Kv1.1 in heterotetramers, which could explain the dominant-negative effects of the V408A Kv1.1 channels (Imbrici et al., 2011). T226K Kv1.1 channels in EA1 also showed a dominant-negative effect when co-expressed in oocytes with the WT Kv1.1 (Chen et al., 2007). In addition, Kv1.1-containing channels in the mammalian central nervous system co-assembled with Kv1.2 and Kv1.4 subunits, which may be also interrupted by the cell-surface expressed mutated Kv1.1 subunit in heterotetramers (D'Adamo et al., 1999; Imbrici et al., 2006). The dominant-negative effects of the V408A Kv1.1 channels in knockin mice as well as S309T Kv1.1 channels in ADMS rats may explain the lethality of the homozygous animals, which are different from that of knockout and *mceph* mice.

In conclusion, using an ENU mutagenesis approach, we have generated *Kcna1*-mutant rats that dominantly express persistent myokymia, neuromyotonia, stress-induced motor incoordination and spontaneous convulsive seizures, as the first rat model of human EA1. The ADMS rat provides a useful animal model of human EA1 to understand the underlying mechanisms of the various clinical phenotypes of *KCNA1*-associated diseases.

4. Experimental procedures

4.1. *Rats and ENU mutagenesis*

Male F344/NSlc (F344) rats (Japan SLC, Hamamatsu, Japan) received two intraperitoneal (i.p.) injections of the chemical mutagen ENU (40 mg/kg) as previously described (Mashimo et al., 2008). Ten weeks after the second ENU injection, males were bred to untreated F344 females to generate ENU-mutagenized G1 progeny (mean mutation frequency: approximately 1 in 4 million base pairs). One female exhibiting muscle twitching and epileptic seizures, was identified and classified as an "affected" founder, then backcrossed to a F344 background, for ten generations (N2–N10), to remove latent ENU-induced mutations in other chromosomal regions. Heterozygous affected N10 males and females were intercrossed to generate the homozygous mutation.

The animal care and experimental procedures used were approved by the Animal Research Committee, Kyoto University and carried out according to the Regulation on Animal Experimentation at Kyoto University. The ADMS rat has been deposited into the National Bio Resource Project — Rat in Japan (NBPR-Rat No. 0458) and is available from the Project (http://www.anim.med.kyoto-u.ac.jp/nbr).

4.2. *Electromyography (EMG) recording*

Rats at 16 weeks of age were used for electromyography (EMG) recordings from muscles in the forelimb (musculus triceps brachii) and hindlimb (musculus quadriceps femoris). To implant EMG electrodes, rats were anesthetized with pentobarbital sodium (50 mg/kg i.p.). Enamel-coated stainless-steel electrodes (100 μm diameter), were prepared by flexing the electrode into a hair-pin curve, 5 mm from the distal end of the electrode. Electrodes were then hooked onto the bevel edge of a 23 gauge injection needle and inserted into the muscle through the overlying skin. The injection needle was removed, leaving the electrode implanted in the appropriate muscle. Pairs of electrodes were implanted in each muscle, to allow bipolar recording, and a ground electrode was inserted subcutaneously on the back. After recovery from anaesthesia, EMG activity was recorded under freely moving conditions, and combined with behavioural observations made using an amplifier (MEG-6108; Nihon Kohden, Tokyo, Japan) and a thermal alley recorder (RTA-1100; Nihon Kohden). The recorded signals were stored (PowerLab ML845; AD Instruments, Bella Vista, Australia) for analysis.

4.3. *Electroencephalogram (EEG) recording*

Rats at 10–20 weeks of age were anesthetized with pentobarbital sodium (50 mg/kg i.p.), and fixed in a stereotaxic instrument (David Kopf Instruments, Tujunga, USA) for implantation of EEG electrodes. Small holes were made in the skull, and screw electrodes were placed on the surface of the right frontal cortex. Enamel-coated stainless-steel electrodes were implanted in the hippocampus (3.8 mm caudal and 2.0 mm lateral to the bregma, and 2.2 mm from the cortex surface). A reference electrode was implanted on the left frontal cranium. The electrodes were then connected to a miniature plug and fixed to the skull with dental cement. After a 1-week recovery period, animals

with chronically implanted electrodes were placed in a shielded box (40×40×40 cm^3). Under freely moving conditions, continuous EEG recordings were made for 3 h during daytime (light-on), with behavioural observations made using an amplifier (MEG-6108; Nihon Kohden) and a thermal alley recorder (RTA-1100; Nihon Kohden). The recorded signals were stored (PowerLab ML845; AD Instruments) for analysis.

4.4. *Antiepileptic drug testing*

Carbamazepine (Sigma-Aldrich Co., St. Louis, USA) dissolved in polyethylene glycol 400 (PEG 400) was used for drug testing (20 mg/kg i.p.), or saline solution (1 ml/kg i.p.) as control. Five ADMS rats at 16–19 weeks of age were observed for 3 h during daytime (light-on) from 30 min after the administration.

4.5. *Histopathology*

Rats at 16–19 weeks of age were deeply anesthetized with sodium pentobarbital (50 mg/kg i.p.). Brains were removed, post-fixed in Bouin's fixative and paraffin embedded. 4 μm paraffin sections were cut and stained with haematoxylin and eosin to evaluate morphological changes.

4.6. *Genetic mapping of Adms*

We produced a total of 180 (BN/SsNSlc×ADMS)×BN/SsNSlc backcross progeny. Genotyping for the *Adms* locus was performed in rats that exhibited the twitching phenotype at 10–14 weeks of age, since spontaneous seizures were not observed in the backcross progeny until at least 20 weeks of age. To localize the *Adms* locus to a specific chromosomal region, we performed genome-wide scanning on DNA samples using a panel of 121 simple sequence length polymorphism (SSLP) markers that cover all the autosomal chromosomes (Chrs). Genomic DNA was prepared from tail biopsies using an automatic DNA purification system (PI-200; Kurabo, Osaka, Japan). All PCRs were performed for 35 cycles (denaturation at 94 °C for 30 s, annealing at 60 °C for 1 min, and extension at 72 °C for 45 s), using Taq polymerase (Takara Bio, Otsu, Japan). PCR products were examined on 4% agarose gels with ethidium bromide staining.

4.7. *Sequence analysis*

The primers used for sequencing the coding regions of *Kcna1*, *Kcna5*, and *Kcna6* are described in Supplementary Table 1. PCR products from genomic DNA were reacted with BigDye Terminator v3.1 cycle sequencing mix (Applied Biosystems, Foster City, USA), followed by the standard protocol for the Applied Biosystems 3100 DNA Sequencer.

4.8. *Western blotting*

Protein lysates were prepared from P10 rat brain as previously described (Imai et al., 2007). 25 μg of each sample was separated on 10% Bis–Tris polyacrylamide gels and analysed by western blotting using rat KCNA1 (ab32433; Abcam, Cambridge, UK) and β-actin (AC-40; Sigma Aldrich) primary antibodies. Secondary antibodies against rabbit IgG (NA934; GE Healthcare Bio-Sciences, Little Chalfont, UK) and mouse IgG (NA931; GE Healthcare Biosciences) were used, respectively.

4.9. *Swimming tests*

Rats at 5 weeks of age were placed in the middle of a tank (30 cm×60 cm, filled with water to a depth of 20 cm) to swim. The water temperature was 17 or 38 °C, and the swim time was 2 min. After swimming, the rats were placed on a dry platform (room temperature 24 °C) for behavioural observation.

4.10. *Cell culture and transfection*

Rat *Kcna1* is encoded by a single exon, allowing the coding region of wild-type (WT) or S309T mutant *Kcna1* to be PCR amplified from genomic DNA. PCR products were inserted into pGEM-T Easy (Promega, Fitchburg, USA) and sequenced to confirm the presence of the S309T mutation. The full length cDNA for each variant (*Kcna1* WT or S309T), was subcloned into pcDNA3.1(–) (Invitrogen, Carlsbad, USA), for western blot analysis, and pIRES2-EGFP (Clontech, Mountain View, USA) for current recording. mRNA was transcribed in vitro using T7-RNA polymerase and a High Yield Capped RNA transcription kit (EPICENTRE Biotechnologies, Madison, USA).

Human embryonic kidney (HEK) 293 cells were grown to 80% confluence in Dulbecco's modified Eagle's medium supplemented with 10% foetal bovine serum, 50 U/ml penicillin and 50 μg/ml streptomycin at 37 °C. Cells were transfected with Lipofectamine 2000 (Invitrogen). For western blot analysis, cells were transfected with pcDNA3.1(–) containing *Kcna1* WT or S309T cDNAs, and maintained for 24 h before harvesting. For whole-cell current recording, cells were transfected with pIRES2-EGFP containing *Kcna1* WT or S309T cDNAs, then plated on glass coverslips at 10% confluence 24 h after transfection, and maintained for another 24 h.

4.11. *Cell-surface biotinylation*

24 h after transfection, HEK 293 cells in 35 mm tissue culture dishes were washed with PBS-CM (PBS containing 1 mM $MgCl_2$ and 0.1 mM $CaCl_2$), then incubated in 0.8 ml of EZ-Link Sulfo-NHS-biotin solution (1 mg/ml in PBS-CM; Thermo Scientific, Waltham, USA) for 30 min on ice. After washing with ice-cold quenching solution (PBS-CM containing 100 mM glycine), cells were incubated in 1 mL quenching solution for 45 min at 4 °C before harvesting, followed by centrifugation for 6 min at 6000×*g*. Cells were then solubilized on ice in 300 μl RIPA buffer (1% Triton X-100, 0.1% SDS, 150 mM NaCl, 1 mM EDTA and 50 mM Tris, pH 7.5 with HCl) containing 1% protease inhibitor cocktail (Invitrogen). The resulting cell lysate was centrifuged for 20 min at 14000×*g*, and the supernatant collected. UltraLink® immobilized streptavidin (Thermo Scientific) was added to the supernatant at a ratio of 1:6, and then incubated overnight at 4 °C with agitation. Next, samples were centrifuged for 1 min at 5000×*g*, and the resin washed with RIPA buffer, high-salt buffer (0.1% Triton X-100, 500 mM NaCl, 5 mM EDTA, 50 mM Tris, pH 7.4 with HCl), and 50 mM Tris (pH7.4 with HCl). Proteins were eluted from the resin by the addition of LDS sample buffer (Invitrogen).

4.12. *Electrophysiological recording from HEK 293 cells*

Whole-cell currents were recorded at room temperature with an EPC 9 amplifier (HEKA, Lambrecht, Germany). Currents were sampled and analysed with Patchmaster 2.43 software (HEKA). Patch pipettes were made from borosilicate glass capillaries (1.5-mm outer diameter; Narishige, Tokyo, Japan) using a P-87 micropipette puller (Sutter Instruments, Novato, USA). The resistance ranged from 2 to 4 MΩ when filled with pipette solution (138 mM NaCl, 5.4 mM KCl, 1.2 mM $MgCl_2$, 1 mM $CaCl_2$, 10 mM EGTA, 10 mM HEPES, 10 mM glucose, pH 7.3 with NaOH). The recording solution was 138 mM NaCl, 5.4 mM KCl, 1.2 mM $MgCl_2$, 1 mM $CaCl_2$, 10 mM EGTA, 10 mM HEPES, 10 mM glucose, pH 7.3 with NaOH.

4.13. *Electrophysiological recording from* **Xenopus** *oocytes*

Small pieces of ovary were isolated from cold-anesthetized *Xenopus laevis* and incubated in Ca^{2+}-free solution (88 mM NaCl, 1 mM KCl, 0.82 mM $MgSO_4$, 2.4 mM $NaHCO_3$, 7.5 mM Tris, pH 7.4 with HCl), containing 1.5 mg/ml collagenase (Sigma-Aldrich) at 20 °C for 3 h. Stage V and VI oocytes were selected and injected with 25 nl of cRNA solution for each *Kcna1* variant (WT or S309T). The injected oocytes were maintained at 20 °C for 4 days in modified Barth's solution (88 mM NaCl, 1 mM KCl, 0.41 mM $CaCl_2$, 0.33 mM $Ca(NO_3)_2$, 0.82 mM $MgSO_4$, 2.4 mM $NaHCO_3$, 7.5 mM Tris, pH7.4 with HCl), supplemented with 300 μg/ml sodium pyruvate, 10 U/ml penicillin and 10 μg/ml streptomycin. Currents were recorded at 20 °C with an OC-725C amplifier (Warner Instruments, Hamden, USA). Currents were sampled and analysed with a PowerLab 2/25 system (AD Instruments) and Scope 4.0.7 software (AD Instruments). The injected oocytes were voltage-clamped at a holding potential of −60 mV with two intracellular glass electrodes (1–2 MΩ with 3 M KCl), made from borosilicate glass capillaries (1.5-mm outer diameter; Narishige) using a PE-2 puller (Narishige). The recording solution was 115 mM NaCl, 2 mM KCl, 2 mM $CaCl_2$, 2 mM $MgCl_2$, 10 mM HEPES, pH 7.2 with NaOH.

Supplementary materials related to this article can be found online at doi:10.1016/j.brainres.2011.11.023.

Acknowledgments

This work was supported in part by Grant-in-Aid for Scientific Research from the Ministry of Education, Culture, Sports, Science and Technology (16200029 to T.M.); and Industrial Technology Research Grant Program from the New Energy and Industrial Technology Development Organization of Japan (08A02004a to T.M.). We would like to thank Fumi Tagami and Yayoi Kunihiro for technical help, and Masashi Sasa for his helpful consultations.

REFERENCES

Adelman, J.P., Bond, C.T., Pessia, M., Maylie, J., 1995. Episodic ataxia results from voltage-dependent potassium channels with altered functions. Neuron 15, 1449–1454.

Bretschneider, F., Wrisch, A., Lehmann-Horn, F., Grissmer, S., 1999. Expression in mammalian cells and electrophysiological characterization of two mutant Kv1.1 channels causing episodic ataxia type 1 (EA-1). Eur. J. Neurosci. 11, 2403–2412.

Browne, D.L., Gancher, S.T., Nutt, J.G., Brunt, E.R., Smith, E.A., Kramer, P., Litt, M., 1994. Episodic ataxia/myokymia syndrome is associated with point mutations in the human potassium channel gene, KCNA1. Nat. Genet. 8, 136–140.

Browne, D.L., Brunt, E.R., Griggs, R.C., Nutt, J.G., Gancher, S.T., Smith, E.A., Litt, M., 1995. Identification of two new KCNA1 mutations in episodic ataxia/myokymia families. Hum. Mol. Genet. 4, 1671–1672.

Chen, H., von Hehn, C., Kaczmarek, L.K., Ment, L.R., Pober, B.R., Hisama, F.M., 2007. Functional analysis of a novel potassium channel (KCNA1) mutation in hereditary myokymia. Neurogenetics 8, 131–135.

Comu, S., Giuliani, M., Narayanan, V., 1996. Episodic ataxia and myokymia syndrome: a new mutation of potassium channel gene Kv1.1. Ann. Neurol. 40, 684–687.

D'Adamo, M.C., Imbrici, P., Sponcichetti, F., Pessia, M., 1999. Mutations in the KCNA1 gene associated with episodic ataxia type-1 syndrome impair heteromeric voltage-gated K(+) channel function. FASEB J. 13, 1335–1345.

Demos, M.K., Macri, V., Farrell, K., Nelson, T.N., Chapman, K., Accili, E., Armstrong, L., 2009. A novel KCNA1 mutation associated with global delay and persistent cerebellar dysfunction. Mov. Disord. 24, 778–782.

Eunson, L.H., Rea, R., Zuberi, S.M., Youroukos, S., Panayiotopoulos, C.P., Liguori, R., Avoni, P., McWilliam, R.C., Stephenson, J.B., Hanna, M.G., Kullmann, D.M., Spauschus, A., 2000. Clinical, genetic, and expression studies of mutations in the potassium channel gene KCNA1 reveal new phenotypic variability. Ann. Neurol. 48, 647–656.

Gilbert, G.J., Graves, T.D., Kullmann, D.M., 2011. Nongenetic factors influence severity of episodic ataxia type 1 in monozygotic twins. Neurology 76, 490 (author reply 490).

Glasscock, E., Qian, J., Yoo, J.W., Noebels, J.L., 2007. Masking epilepsy by combining two epilepsy genes. Nat. Neurosci. 10, 1554–1558.

Glasscock, E., Yoo, J.W., Chen, T.T., Klassen, T.L., Noebels, J.L., 2010. Kv1.1 potassium channel deficiency reveals brain-driven cardiac dysfunction as a candidate mechanism for sudden unexplained death in epilepsy. J. Neurosci. 30, 5167–5175.

Glaudemans, B., van der Wijst, J., Scola, R.H., Lorenzoni, P.J., Heister, A., van der Kemp, A.W., Knoers, N.V., Hoenderop, J.G., Bindels, R.J., 2009a. A missense mutation in the Kv1.1 voltage-gated potassium channel-encoding gene KCNA1 is linked to human autosomal dominant hypomagnesemia. J. Clin. Invest. 119, 936–942.

Glaudemans, B., van der Wijst, J., Scola, R.H., Lorenzoni, P.J., Heister, A., van der Kemp, A.W., Knoers, N.V., Hoenderop, J.G., Bindels, R.J., 2009b. A missense mutation in the Kv1.1 voltage-gated potassium channel-encoding gene KCNA1 is linked to human autosomal dominant hypomagnesemia. J. Clin. Invest. 119, 936–942.

Graves, T.D., Rajakulendran, S., Zuberi, S.M., Morris, H.R., Schorge, S., Hanna, M.G., Kullmann, D.M., 2010. Nongenetic factors influence severity of episodic ataxia type 1 in monozygotic twins. Neurology 75, 367–372.

Herson, P.S., Virk, M., Rustay, N.R., Bond, C.T., Crabbe, J.C., Adelman, J.P., Maylie, J., 2003. A mouse model of episodic ataxia type-1. Nat. Neurosci. 6, 378–383.

Imai, Y., Inoue, H., Kataoka, A., Hua-Qin, W., Masuda, M., Ikeda, T., Tsukita, K., Soda, M., Kodama, T., Fuwa, T., Honda, Y., Kaneko, S., Matsumoto, S., Wakamatsu, K., Ito, S., Miura, M., Aosaki, T., Itohara, S., Takahashi, R., 2007. Pael receptor is involved in dopamine metabolism in the nigrostriatal system. Neurosci. Res. 59, 413–425.

Imbrici, P., D'Adamo, M.C., Kullmann, D.M., Pessia, M., 2006. Episodic ataxia type 1 mutations in the KCNA1 gene impair the fast inactivation properties of the human potassium channels

Kv1.4-1.1/Kvbeta1.1 and Kv1.4-1.1/Kvbeta1.2. Eur. J. Neurosci. 24, 3073–3083.

Imbrici, P., Gualandi, F., D'Adamo, M.C., Masieri, M.T., Cudia, P., De Grandis, D., Mannucci, R., Nicoletti, I., Tucker, S.J., Ferlini, A., Pessia, M., 2008. A novel KCNA1 mutation identified in an Italian family affected by episodic ataxia type 1. Neuroscience 157, 577–587.

Imbrici, P., D'Adamo, M.C., Grottesi, A., Biscarini, A., Pessia, M., 2011. Episodic ataxia type 1 mutations affect fast inactivation of K^+ channels by a reduction in either subunit surface expression or affinity for inactivation domain. Am. J. Physiol. Cell Physiol. 300, C1314–C1322.

Johnston, J., Forsythe, I.D., Kopp-Scheinpflug, C., 2010. Going native: voltage-gated potassium channels controlling neuronal excitability. J. Physiol. 588, 3187–3200.

Kinali, M., Jungbluth, H., Eunson, L.H., Sewry, C.A., Manzur, A.Y., Mercuri, E., Hanna, M.G., Muntoni, F., 2004. Expanding the phenotype of potassium channelopathy: severe neuromyotonia and skeletal deformities without prominent Episodic Ataxia. Neuromuscul. Disord. 14, 689–693.

Klein, A., Boltshauser, E., Jen, J., Baloh, R.W., 2004. Episodic ataxia type 1 with distal weakness: a novel manifestation of a potassium channelopathy. Neuropediatrics 35, 147–149.

Knight, M.A., Storey, E., McKinlay Gardner, R.J., Hand, P., Forrest, S.M., 2000. Identification of a novel missense mutation L329I in the episodic ataxia type 1 gene KCNA1—a challenging problem. Hum. Mutat. 16, 374.

Kopp-Scheinpflug, C., Fuchs, K., Lippe, W.R., Tempel, B.L., Rubsamen, R., 2003. Decreased temporal precision of auditory signaling in Kcna1-null mice: an electrophysiological study in vivo. J. Neurosci. 23, 9199–9207.

Lee, H., Wang, H., Jen, J.C., Sabatti, C., Baloh, R.W., Nelson, S.F., 2004. A novel mutation in KCNA1 causes episodic ataxia without myokymia. Hum. Mutat. 24, 536.

Lopantsev, V., Tempel, B.L., Schwartzkroin, P.A., 2003. Hyperexcitability of CA3 pyramidal cells in mice lacking the potassium channel subunit Kv1.1. Epilepsia 44, 1506–1512.

Mashimo, T., Yanagihara, K., Tokuda, S., Voigt, B., Takizawa, A., Nakajima, R., Kato, M., Hirabayashi, M., Kuramoto, T., Serikawa, T., 2008. An ENU-induced mutant archive for gene targeting in rats. Nat. Genet. 40, 514–515.

Mashimo, T., Ohmori, I., Ouchida, M., Ohno, Y., Tsurumi, T., Miki, T., Wakamori, M., Ishihara, S., Yoshida, T., Takizawa, A., Kato, M., Hirabayashi, M., Sasa, M., Mori, Y., Serikawa, T., 2010. A missense mutation of the gene encoding voltage-dependent sodium channel (Nav1.1) confers susceptibility to febrile seizures in rats. J. Neurosci. 30, 5744–5753.

Persson, A.S., Klement, G., Almgren, M., Sahlholm, K., Nilsson, J., Petersson, S., Arhem, P., Schalling, M., Lavebratt, C., 2005. A truncated Kv1.1 protein in the brain of the megencephaly mouse: expression and interaction. BMC Neurosci. 6, 65.

Pessia, M., Hanna, M.G., 1993. Episodic Ataxia Type 1. Vol. In: Pagon, R.A., Bird, T.D., Dolan, C.R., Stephens, K. (Eds.), GeneReviews. University of Washington, Seattle, Seattle WA (Vol.).

Petersson, S., Persson, A.S., Johansen, J.E., Ingvar, M., Nilsson, J., Klement, G., Arhem, P., Schalling, M., Lavebratt, C., 2003. Truncation of the Shaker-like voltage-gated potassium channel, Kv1.1, causes megencephaly. Eur. J. Neurosci. 18, 3231–3240.

Poujois, A., Antoine, J.C., Combes, A., Touraine, R.L., 2006. Chronic neuromyotonia as a phenotypic variation associated with a new mutation in the KCNA1 gene. J. Neurol. 253, 957–959.

Rajakulendran, S., Schorge, S., Kullmann, D.M., Hanna, M.G., 2007. Episodic ataxia type 1: a neuronal potassium channelopathy. Neurotherapeutics 4, 258–266.

Rho, J.M., Szot, P., Tempel, B.L., Schwartzkroin, P.A., 1999. Developmental seizure susceptibility of kv1.1 potassium channel knockout mice. Dev. Neurosci. 21, 320–327.

Scheffer, H., Brunt, E.R., Mol, G.J., van der Vlies, P., Stulp, R.P., Verlind, E., Mantel, G., Averyanov, Y.N., Hofstra, R.M., Buys, C.H., 1998. Three novel KCNA1 mutations in episodic ataxia type I families. Hum. Genet. 102, 464–466.

Schulte, U., Thumfart, J.O., Klocker, N., Sailer, C.A., Bildl, W., Biniossek, M., Dehn, D., Deller, T., Eble, S., Abbass, K., Wangler, T., Knaus, H.G., Fakler, B., 2006. The epilepsy-linked Lgi1 protein assembles into presynaptic Kv1 channels and inhibits inactivation by Kvbeta1. Neuron 49, 697–706.

Shook, S.J., Mamsa, H., Jen, J.C., Baloh, R.W., Zhou, L., 2008. Novel mutation in KCNA1 causes episodic ataxia with paroxysmal dyspnea. Muscle Nerve 37, 399–402.

Smart, S.L., Lopantsev, V., Zhang, C.L., Robbins, C.A., Wang, H., Chiu, S.Y., Schwartzkroin, P.A., Messing, A., Tempel, B.L., 1998. Deletion of the K(V)1.1 potassium channel causes epilepsy in mice. Neuron 20, 809–819.

Tomlinson, S.E., Tan, S.V., Kullmann, D.M., Griggs, R.C., Burke, D., Hanna, M.G., Bostock, H., 2010. Nerve excitability studies characterize Kv1.1 fast potassium channel dysfunction in patients with episodic ataxia type 1. Brain 133, 3530–3540.

Wenzel, H.J., Vacher, H., Clark, E., Trimmer, J.S., Lee, A.L., Sapolsky, R.M., Tempel, B.L., Schwartzkroin, P.A., 2007. Structural consequences of Kcna1 gene deletion and transfer in the mouse hippocampus. Epilepsia 48, 2023–2046.

Wulff, H., Castle, N.A., Pardo, L.A., 2009. Voltage-gated potassium channels as therapeutic targets. Nat. Rev. Drug Discov. 8, 982–1001.

Yoshimi, K., Tanaka, T., Takizawa, A., Kato, M., Hirabayashi, M., Mashimo, T., Serikawa, T., Kuramoto, T., 2009. Enhanced colitis-associated colon carcinogenesis in a novel Apc mutant rat. Cancer Sci. 100, 2022–2027.

Zerr, P., Adelman, J.P., Maylie, J., 1998. Characterization of three episodic ataxia mutations in the human Kv1.1 potassium channel. FEBS Lett. 431, 461–464.

Zhang, C.L., Messing, A., Chiu, S.Y., 1999. Specific alteration of spontaneous GABAergic inhibition in cerebellar purkinje cells in mice lacking the potassium channel Kv1. 1. J. Neurosci. 19, 2852–2864.

Zhou, L., Zhang, C.L., Messing, A., Chiu, S.Y., 1998. Temperature-sensitive neuromuscular transmission in Kv1.1 null mice: role of potassium channels under the myelin sheath in young nerves. J. Neurosci. 18, 7200–7215.

Zuberi, S.M., Eunson, L.H., Spauschus, A., De Silva, R., Tolmie, J., Wood, N.W., McWilliam, R.C., Stephenson, J.B., Kullmann, D.M., Hanna, M.G., 1999. A novel mutation in the human voltage-gated potassium channel gene (Kv1.1) associates with episodic ataxia type 1 and sometimes with partial epilepsy. Brain 122 (Pt 5), 817–825.

Human Molecular Genetics, 2012, Vol. 21, No. 16 **3546–3557**
doi:10.1093/hmg/dds184
Advance Access published on May 15, 2012

A rat model for LGI1-related epilepsies

Stéphanie Baulac[1,2,3,*,†], Saeko Ishida[5,†], Tomoji Mashimo[5,*], Morgane Boillot[1,2,3], Naohiro Fumoto[5,6], Mitsuru Kuwamura[7], Yukihiro Ohno[8], Akiko Takizawa[5], Toshihiro Aoto[9], Masatsugu Ueda[9], Akio Ikeda[6], Eric LeGuern[1,2,3,4], Ryosuke Takahashi[6] and Tadao Serikawa[5]

[1]Inserm U975, CRICM, [2]Université Pierre and Marie Curie-Paris 6, UMR_S975, [3]CNRS, UMR7225 and [4]AP-HP, Département de Génétique et Cytogénétique, Centre de génétique moléculaire et chromosomique, Hôpital de la Pitié-Salpêtrière, Paris F-75013, France, [5]Institute of Laboratory Animals, Graduate School of Medicine and [6]Department of Neurology, Graduate School of Medicine, Kyoto University, Kyoto 606-8501, Japan, [7]Laboratory of Veterinary Pathology, Osaka Prefecture University, Izumisano, Osaka 598-8531, Japan, [8]Laboratory of Pharmacology, Osaka University of Pharmaceutical Sciences, Takatsuki 569-1094, Japan and [9]PhoenixBio Co. Ltd, Utsunomiya 321-0973, Japan

Received March 20, 2012; Revised and Accepted May 10, 2012

Mutations of the leucine-rich glioma-inactivated 1 (*LGI1*) gene cause an autosomal dominant partial epilepsy with auditory features also known as autosomal-dominant lateral temporal lobe epilepsy. LGI1 is also the main antigen present in sera and cerebrospinal fluids of patients with limbic encephalitis and seizures, highlighting its importance in a spectrum of epileptic disorders. *LGI1* encodes a neuronal secreted protein, whose brain function is still poorly understood. Here, we generated, by ENU (*N*-ethyl-*N*-nitrosourea) mutagenesis, *Lgi1*-mutant rats carrying a missense mutation (L385R). We found that the L385R mutation prevents the secretion of Lgi1 protein by COS7 transfected cells. However, the L385R-Lgi1 protein was found at low levels in the brains and cultured neurons of *Lgi1*-mutant rats, suggesting that mutant protein may be destabilized *in vivo*. Studies on the behavioral phenotype and intracranial electroencephalographic signals from *Lgi1*-mutant rats recalled several features of the human genetic disorder. We show that homozygous *Lgi1*-mutant rats (*Lgi1*$^{L385R/L385R}$) generated early-onset spontaneous epileptic seizures from P10 and died prematurely. Heterozygous *Lgi1*-mutant rats (*Lgi1*$^{+/L385R}$) were more susceptible to sound-induced, generalized tonic-clonic seizures than control rats. Audiogenic seizures were suppressed by antiepileptic drugs such as carbamazepine, phenytoin and levetiracetam, which are commonly used to treat partial seizures, but not by the prototypic absence seizure drug, ethosuximide. Our findings provide the first rat model with a missense mutation in *Lgi1* gene, an original model complementary to knockout mice. This study revealed that *LGI1* disease-causing missense mutations might cause a depletion of the protein in neurons, and not only a failure of Lgi1 secretion.

INTRODUCTION

Epilepsy, with a lifetime prevalence of 3%, is a frequent neurological disorder. Studies on familial idiopathic epilepsies have identified multiple disease-causing genes (1). For example, mutations in the leucine-rich glioma-inactivated 1 (*LGI1*) gene cause an inherited epilepsy syndrome designated either autosomal dominant lateral temporal epilepsy (ADLTE) (2) or autosomal dominant partial epilepsy with auditory features (3). Focal seizures, with prominent auditory auras in about two thirds of patients, emerge in adolescence (4). Aphasic symptoms and other aberrant perceptions of a visual, vertiginous, epigastric or psychogenic nature are also

*To whom correspondence should be addressed at: Institute of Laboratory Animals, Graduate School of Medicine, Kyoto University, Yoshidakonoe-cho, Sakyo-ku, Kyoto 606-8501, Japan. Tel: +81-75-753-9318; Fax: +81-75-753-4409; Email: tmashimo@anim.med.kyoto-u.ac.jp (T.M.); Institut du Cerveau et de la Moelle épinière (ICM), Hôpital de la Pitié -Salpêtrière - 47, bd de l'hôpital, 75013 Paris, France. Tel: +33-1-57-27-43-39; Fax: +33-1-57-27-40-27; Email: stephanie.baulac@upmc.fr (S.B.)
†Authors contributed equally to this study.

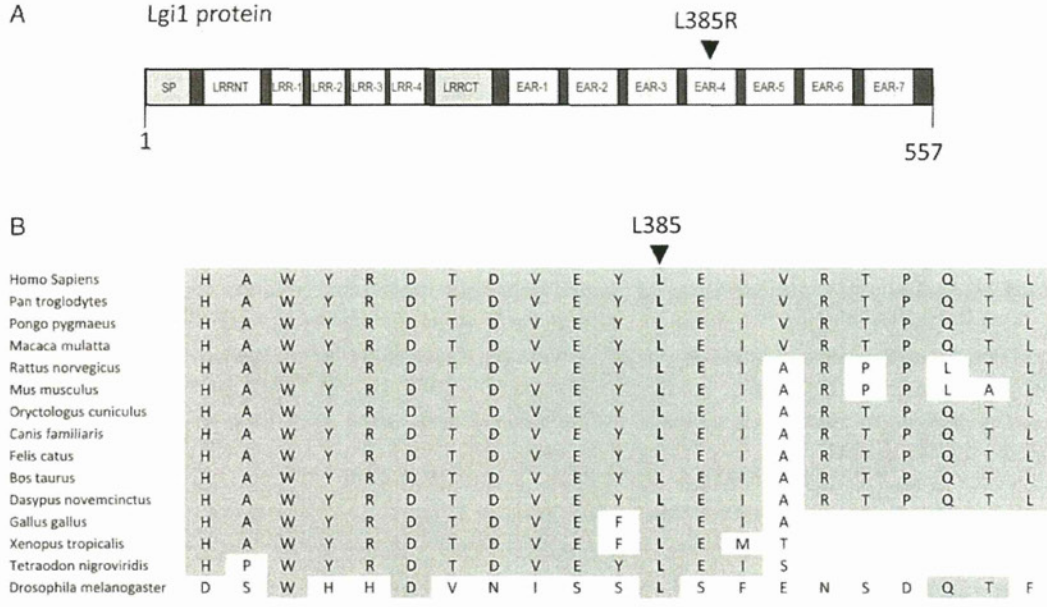

Figure 1. The L385R mutation. (**A**) Schematic representation of the Lgi1 protein showing its domain organization and location of the L385R mutation. The protein is composed of two structural domains: four N-terminal LRR (in blue) and seven EAR (in yellow) in the C-terminal half of the protein. (**B**) Multiple protein alignments of Lgi1 protein showing the strong conservation of L385 residue in both vertebrates and invertebrates using the Alamut® Mutation Interpretation Software.

reported, and seizures can be triggered by noises or voices (5,6). *LGI1* mutations (36 published to date) (7) have been found in up to 50% of ADLTE families and 2% of sporadic cases (8). The role of LGI1 in neurological diseases was further expanded with the recent discovery that a subset of patients with limbic encephalitis (an autoimmune disorder associated with seizures in the majority of patients) (9,10) has serum antibodies against LGI1. It is speculated that the antibody-mediated disruption of LGI1 causes increased excitability, which results in seizures and other symptoms of limbic encephalopathy (11).

In contrast to other genes linked to idiopathic epilepsies, *LGI1* does not encode an ion channel subunit, but rather a secreted leucine-rich repeat (LRR) protein (12). Except R407C (13), all tested *LGI1* missense mutations tend to suppress protein secretion in *in vitro* overexpression systems (12,14–18), indicating that extracellular levels of LGI1 may be critical to its pathophysiological effects. Lgi1 protein is expressed during mouse embryogenesis and increases until adult, suggesting that it may have a role during brain development (19–21). While its functions remain unclear, Lgi1 interacts with the presynaptic Kv1.1 voltage-gated potassium channel (22), ADAM22/ADAM23 (disintegrin and metalloproteinase domains 22 and 23) (23), ADAM11 (24) and NogoR1 (25). Insights into the role of Lgi1 in epilepsy have emerged from three recent studies on *Lgi1* knockout ($Lgi1^{-/-}$) in mice. There is a consensus that in homozygous $Lgi1^{-/-}$ mice, the constitutive deletion of *Lgi1* induces early-onset spontaneous seizures followed by premature death (20,26,27). Heterozygous $Lgi1^{+/-}$ mice do not generate seizures spontaneously, but they are more prone to seizure induction by pentylenetetrazole (26) and auditory stimuli (20). Lgi1 may cause epilepsy by modulating signaling in glutamatergic (21,26,27) but not GABAergic synaptic circuits (21,27). However, the two studies of $Lgi1^{-/-}$ brain slices contradict each other, suggesting that the loss of Lgi1 either reduces (26) or increases (27) alpha-amino-3-hydroxy-5-méthylisoazol-4-propionate-mediated miniature excitatory post-synaptic currents in CA1 hippocampal neurons. An alternative pathophysiological mechanism might be that Lgi1 controls the postnatal maturation of glutamatergic synapses in the hippocampus (21) and retinogeniculate thalamic afferents (28).

In the present study, we generated and characterized *Lgi1*-mutant rats carrying a missense mutation (L385R). We deciphered the mechanisms by which this mutation led to a loss of function in transfected mammalian cells and primary neurons in culture. Electroencephalographic (EEG) monitoring was used to define how the L385R-Lgi1 protein affected the phenotype of homozygous and heterozygous *Lgi1*-mutant rats *in vivo*. Finally, we examined actions of antiepileptic drugs on the audiogenic seizures in heterozygous $Lgi1^{+/L385R}$ rats.

RESULTS

Generation of *Lgi1*-mutant rats

The ENU (*N*-ethyl-*N*-nitrosourea)-mutagenized F344/NSlc rat archive (KURMA: Kyoto University Rat Mutant Archive) was screened for mutations in the *Lgi1* gene by a high-throughput screening assay (29). A missense mutation (c.1154 T > G) in exon 8 of *Lgi1* was found in one DNA sample of KURMA. This mutation resulted in the p.Leu385Arg/L385R amino acid substitution in the fourth epilepsy-associated repeat

(EAR; Fig. 1A), a residue highly conserved among vertebrates and invertebrates (Fig. 1B). Four bioinformatics prediction programs of functional effects of variants were queried for L385R. All predicted a significant effect of this amino acid change on protein function: 'not tolerated' by SIFT (http://sift.bii.a-star.edu.sg/), 'disease causing' by Mutation taster (http://www.mutationtaster.org/), 'probably damaging' by PolyPhen-2 (http://genetics.bwh.harvard.edu/pph2) and a P-deleterious of 0.991 by Panther (http://www.pantherdb.org/). Interestingly, a well-documented ADLTE-causing mutation, p.Glu383Ala/E383A, was located close to the Rat mutation (3,12,14). The heterozygous *Lgi1*-mutant rat ($Lgi1^{+/L385R}$) was recovered from the corresponding frozen sperm by intracytoplasmic sperm injection. Nine generations were backcrossed on the F344/NSIc inbred background to eliminate mutations potentially induced by ENU mutagenesis elsewhere in the genome (mean mutation frequency was ~1 in 4×10^6 bp). Backcrossed $Lgi1^{+/L385R}$ rats were then intercrossed to obtain wild-type (WT; $Lgi1^{+/+}$), heterozygous ($Lgi1^{+/L385R}$) and homozygous ($Lgi1^{L385R/L385R}$) animals. They were born in expected Mendelian ratios ($Lgi1^{+/+}$, $n = 17$; $Lgi1^{L385R/L385R}$, $n = 18$; $Lgi1^{+/L385R}$, $n = 29$; $\chi^2 = 0.59$, not significant) and sex ratios ($Lgi1^{L385R/L385R}$ rats: 28 females and 36 males; $\chi^2 = 1$, not significant).

L385R mutation impairs Lgi1 secretion in COS7 cells and cortical neurons

We asked whether the rat L385R mutation impaired Lgi1 secretion, by transiently transfecting COS7 cells with Flag-Lgi1-L385R, Flag-Lgi1-E383A or Flag-Lgi1-WT. Using an antibody directed against amino acids 200–300 of Lgi1 (ab30868), western blot analysis revealed the presence of WT Lgi1 and both mutants in the cell lysates. However, while WT Lgi1 protein was predominantly present in the cell culture medium, we did not detect the Flag-Lgi1-L385R or the Flag-Lgi1-E383A mutants (Fig. 2A). This shows that the L385R mutation prevents the secretion of Lgi1 into the culture medium of COS7 cells.

We next examined endogenous Lgi1 secretion in isolated neurons of primary cortical cultures from rat embryonic day 19 (E19) $Lgi1^{L385R/L385R}$, $Lgi1^{+/L385R}$ and $Lgi1^{+/+}$ littermates. Western blot analysis revealed only weak signal of 65 kDa in the neuron lysate of homozygous $Lgi1^{L385R/L385R}$ rats, as well as in the neuron medium, indicating a low level of L385R-Lgi1 protein in neurons (Fig. 2B).

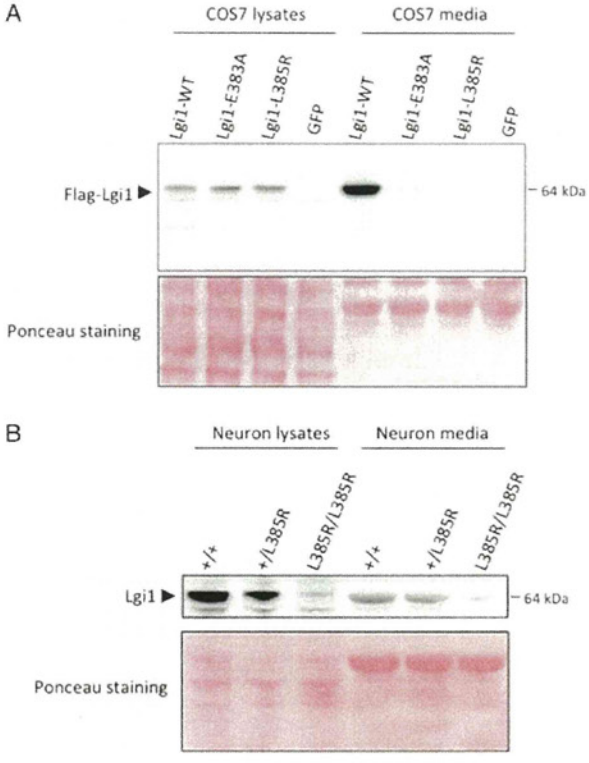

Figure 2. Lack of secretion of L385R-Lgi1 mutant protein in COS7 cells and cortical neurons. (**A**) COS7 cells were transiently transfected with the WT or indicated mutant Flag-Lgi1-expressing plasmids. Cell lysates and cell media were analyzed by western blot with an anti-Lgi1 antibody (ab30868). Lgi1-WT was detected in both the lysate and the culture media, while Lgi1-L385R and Lgi1-E383A mutants were only detected in the cell lysates. (**B**) Cortical and hippocampal E19 neurons from $Lgi1^{+/+}$, $Lgi1^{+/L385R}$ and $Lgi1^{L385R/L385R}$ littermate rats were cultured. Cell lysates and media were analyzed by western blot with an anti-Lgi1 antibody (ab30868). L385R-Lgi1 mutant protein was weakly detected in both the lysates and the culture media, in contrast to the WT Lgi1 protein. Ponceau staining indicated equal loading in each well.

L385R-Lgi1 is unstable *in vivo*

We then compared the endogenous L385R-Lgi1 protein level by western blot in whole brain homogenates of postnatal day 12 (P12) $Lgi1^{L385R/L385R}$, $Lgi1^{+/L385R}$ and WT ($Lgi1^{+/+}$) littermate rats. Immunoblot revealed a single band of 65 kDa in the lysate of $Lgi1^{+/+}$. It was reduced by about half in $Lgi1^{+/L385R}$ and was absent in $Lgi1^{L385R/L385R}$ ($n = 5$; Fig. 3A). The low abundance of L385R-Lgi1 protein in the brain was confirmed with a second antibody generated to the C terminus of Lgi1 (sc-9583, Santa Cruz; Supplementary Material, Fig. 1S). These findings were replicated in three additional litters of WT, heterozygous and homozygous rats aged P5 and P9 (before onset of seizures) and P12 (after onset of seizures), indicating that lack of L385R-Lgi1 was not secondary to seizures (data not shown). We next analyzed synaptic fractions of hippocampal and cortical lysates by preparing Triton X-100 crude fractions. A strong signal was detected in $Lgi1^{+/+}$ and $Lgi1^{+/L385R}$ lysates, indicating that WT Lgi1 protein was present in the synapse-enriched fraction. In contrast, only a very weak band was detected for L385R-Lgi1 protein in the Triton X-100-insoluble membrane synaptic fraction (Fig. 3B), suggesting that it is probably unstable and thus not delivered to the synapse.

We next asked whether low levels of L385R-Lgi1 protein resulted from a preferential degradation of the L385R-*Lgi1* transcript. We extracted total RNAs from the whole brains of $Lgi1^{L385R/L385R}$ ($n = 5$), $Lgi1^{+/L385R}$ ($n = 7$) and $Lgi1^{+/+}$ ($n = 5$) littermate rats and analyzed *Lgi1* transcript expression by quantitative reverse transcription (RT)–polymerase chain reaction (PCR). Relative levels of the L385R-*Lgi1* transcript were not significantly different from levels of the $Lgi1^{+/+}$ transcript (Kruskal–Wallis test, not significant; Fig. 3C).

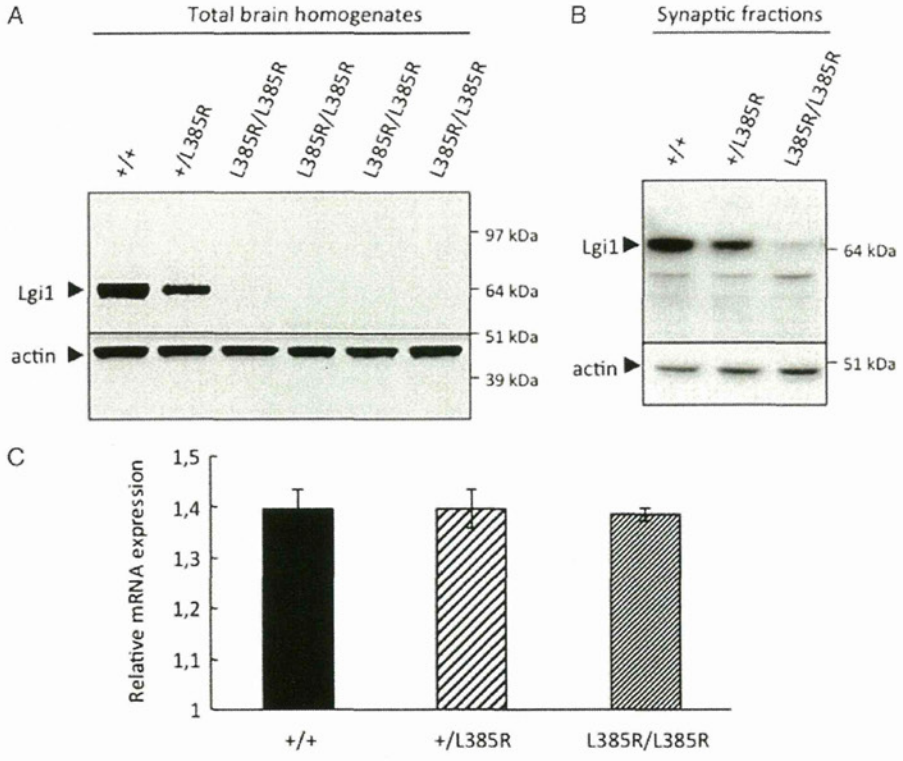

Figure 3. Instability of the L385R-Lgi1 mutant protein. (**A**) We assessed Lgi1 protein expression by western blot of whole brain lysates of $Lgi1^{+/+}$ ($n = 1$), $Lgi1^{+/L385R}$ ($n = 1$) and $Lgi1^{L385R/L385R}$ ($n = 5$) P12 littermate rats. WT Lgi1 protein was detected, but not L385R-Lgi1. Equal amounts of proteins were loaded as shown by the actin control. (**B**) Synaptic-enriched fraction lysates from $Lgi1^{+/+}$ ($n = 1$), $Lgi1^{+/L385R}$ ($n = 1$) and $Lgi1^{L385R/L385R}$ ($n = 1$) littermate rats aged P12. L385R-Lgi1 mutant protein was only weakly detected. (**C**) Quantitative PCR on total cDNAs of $Lgi1^{+/+}$ ($n = 5$), $Lgi1^{+L385R}$ ($n = 6$) and $Lgi1^{L385R/L385R}$ ($n = 6$) rat brains. Data are the mean ± SD of triplicates (P not significant) corresponding to the expression of *Lgi1* transcript in relation to the housekeeping gene PPIA.

These results suggest that low neuronal levels of L385R-Lgi1 protein may result from a shortened half-life of the protein rather than the transcript.

L385R mutation has no major effect on *in vitro* neuronal growth

We asked whether this L385R mutation affected the growth of primary neurons plated on poly-L-lysine coated culture plates. Cortical and hippocampal neurons from E19 rats were co-cultured for 3 weeks and examined daily. No differential effect on life span or neurite outgrowth was detected between $Lgi1^{L385R/L385R}$ and $Lgi1^{+/+}$ rats (ImageJ measurement of total neurite network length, Kruskal–Wallis test, not significant; Fig. 4A). In addition, no major morphological differences were detected between hematoxylin-stained brains of P12 $Lgi1^{L385R/L385R}$ rats and their $Lgi1^{+/L385R}$ and $Lgi1^{+/+}$ littermates (Fig. 4B).

Homozygous *Lgi1*-mutant rats are epileptic and die prematurely

At birth, we detected no differences in appearance or behavior of homozygous $Lgi1^{L385R/L385R}$ rats and heterozygous $Lgi1^{+/L385R}$ or $Lgi1^{+/+}$ littermates. During the second postnatal week, $Lgi1^{L385R/L385R}$ pups began to exhibit spontaneous seizures (Fig. 5A, Supplementary Material, Movie S1). They occurred from P10 at a mean frequency of 8 ± 2.8 per hour (mean ± SD, $n = 8$) with a mean duration of 83 ± 4.9 s. Ictal epileptic discharges ($n = 11$ electroclinical seizures) were recorded by intracranial EEG in two homozygous $Lgi1^{L385R/L385R}$ pups (Fig. 5B). Seizures typically consisted of sequences of (i) hypertonic, often asymmetric, trunk, limb and tail postures, (ii) clonies of all limbs or jerking. EEG records began with rhythmic 5–7 Hz spike activity, which increased in amplitude. It was replaced by polyspike-and-wave complexes at 1 Hz during jerking episodes which slowed (0.5 Hz) as the seizure terminated. Seizures were sometimes associated with motor automatisms, such as chewing. Such spontaneous epileptic activity was never observed in age-matched heterozygous $Lgi1^{+/L385R}$ ($n = 7$) or $Lgi1^{-/+}$ littermates ($n = 7$).

As seizures emerged, $Lgi1^{L385R/L385R}$ rat pups failed to gain weight. At P15, the average body weight of $Lgi1^{L385R/L385R}$ rats was significantly (pairwise Student's t-test, $P < 0.009$) lower than that of $Lgi1^{+/L385R}$ or $Lgi1^{+/+}$ rats (respectively, 10.4, 25 and 24 g; Fig. 6A), and development slowed dramatically (Fig. 6B). All homozygous $Lgi1^{L385R/L385R}$ rats died prematurely and the Kaplan–Meier curve revealed a mean lifetime of 13 days ($n = 10$). No homozygous $Lgi1^{L385R/L385R}$ rat

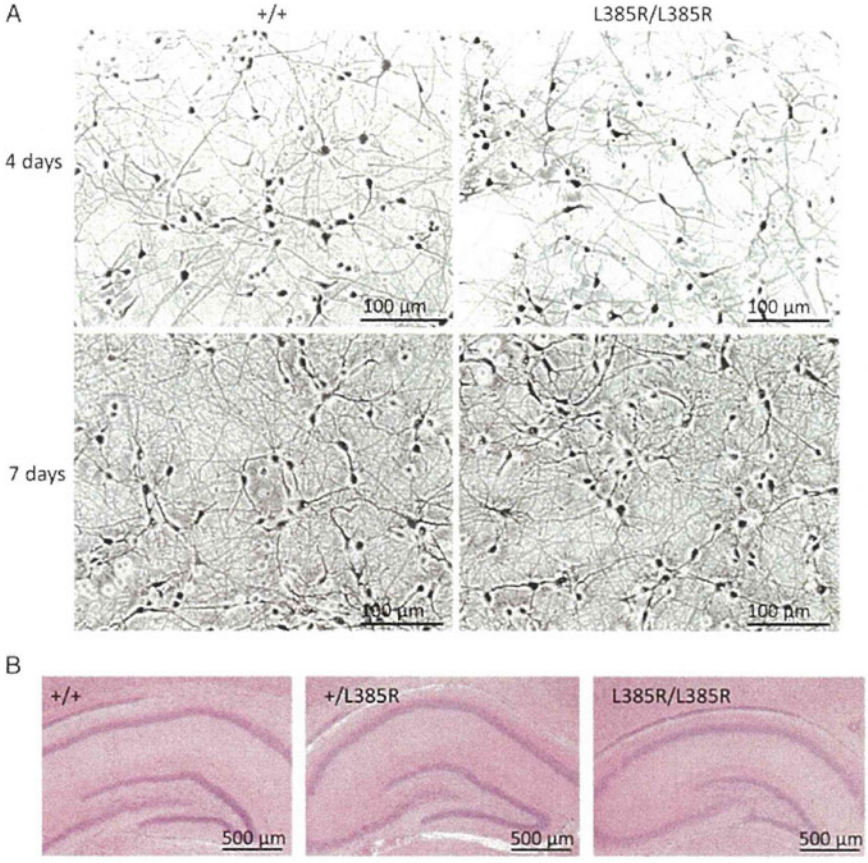

Figure 4. No major effect of L385R mutation on neuronal growth. (**A**) Photography of cortical neurons from E19 $Lgi1^{+/+}$ ($n = 2$) and $Lgi1^{L385R/L385R}$ ($n = 6$) littermate rats after 4 or 7 days in culture. We observed no major difference on the length of neurites or survival in $Lgi1^{L385R/L385R}$ rats compared with $Lgi1^{+/+}$ littermates. Background was subtracted using ImageJ. (**B**) Hematoxylin and eosin-stained coronal brain sections show the similar morphology of dentate gyrus in $Lgi1^{+/+}$ ($n = 1$), $Lgi1^{+/L385R}$ ($n = 1$) and $Lgi1^{L385R/L385R}$ ($n = 1$) littermates aged P12.

survived beyond P17, while no $Lgi1^{+/L385R}$ or $Lgi1^{+/+}$ littermates had died at this age (Fig. 6C). Possibly, this early mortality results from a failure to feed due to seizures.

Heterozygous *Lgi1*-mutant rats display increased audiogenic seizure vulnerability

Heterozygous $Lgi1^{+/L385R}$ rats appear normal, are fertile and live for at least 1 year. Spontaneous clinical seizures have never been observed in either pups or adults. Since partial seizures can be triggered by audiogenic events in ADLTE patients, we tested the susceptibility of heterozygous *Lgi1*-mutant rats to audiogenic seizures. A single 120-dB sound stimulus at 10 kHz never induced seizures in $Lgi1^{+/L385R}$ or $Lgi1^{+/+}$ rats at 3, 5, 8 or 12 weeks of age, possibly due to this rat strain resistance to audiogenic seizures. Acoustic priming (5 min, 10 kHz, 120 dB) was thus applied to rat pups aged P16, corresponding to the critical period when rats become seizure prone (30). Primed rats were then tested for audiogenic seizures at 8 weeks of age. Auditory stimulus first induced wild running, a typical behavior of audiogenic seizures, in all $Lgi1^{+/L385R}$ ($n = 22$) and $Lgi1^{+/+}$ ($n = 14$) rats (Table 1). Following wild running, auditory stimulation yielded generalized tonic-clonic seizures (GTCSs) in all $Lgi1^{+/L385R}$ rats, but only in 4 of 14 (28%) $Lgi1^{+/+}$ rats ($\chi^2 = 22$, $P = 3 \times 10^{-6}$; Fig. 7A, Supplementary Material, Movie S2). The latency from auditory stimulus to wild running was shorter in $Lgi1^{+/L385R}$ than $Lgi1^{+/+}$ rats (Student's *t*-test, $P = 2.7 \times 10^{-2}$; Fig. 7B). The duration of wild running was also shorter in $Lgi1^{+/L385R}$ than in $Lgi1^{+/+}$ rats (Student's *t*-test, $P = 6.8 \times 10^{-5}$; Fig. 7C), probably since wild running was more rapidly replaced by a GTCS in $Lgi1^{+/L385R}$ rats. The duration of GTCSs did not differ significantly in $Lgi1^{+/L385R}$ and $Lgi1^{+/+}$ rats (Student's *t*-test, $P = 4.5 \times 10^{-1}$; Fig. 7D).

We compared cortical and hippocampal EEG signals generated by $Lgi1^{+/L385R}$ ($n = 3$) and $Lgi1^{+/+}$ ($n = 1$) rats during auditory stimuli (Fig. 8). During wild running, movement artifacts tended to obscure EEG signals. After running terminated, EEG signals were strongly suppressed in the tonic phase of $Lgi1^{+/L385R}$ rats and the immobility phase of $Lgi1^{+/+}$ rats. During the clonic seizure phase in $Lgi1^{+/L385R}$ rats, continuous rhythmic slow activity at 2–3 Hz was detected in cortex and hippocampus. EEG signals were then suppressed, as $Lgi1^{+/L385R}$ rats remained immobile until auditory stimuli ceased.